

Power System Dynamics as Primal-Dual Algorithm for Optimal Load Control

Changhong Zhao*, Ufuk Topcu[†], Na Li[‡] and Steven H. Low*

*Electrical Engineering, California Institute of Technology

{czhao, slow}@caltech.edu

[†] Electrical & Systems Engineering, University of Pennsylvania

utopcu@seas.upenn.edu

[‡] Control and Dynamical Systems, California Institute of Technology

nali@caltech.edu

Abstract

We formulate an optimal load control (OLC) problem in power networks where the objective is to minimize the aggregate cost of tracking an operating point subject to power balance over the network. We prove that the swing dynamics and the branch power flows, coupled with frequency-based load control, serve as a distributed primal-dual algorithm to solve OLC. Even though the system has multiple equilibrium points, we prove that it nonetheless converges to an optimal point. This result implies that the local frequency deviations at each bus convey exactly the right information about the global power imbalance for the loads to make individual decisions that turn out to be globally optimal. It allows a completely decentralized solution without explicit communication among the buses. Simulations show that the proposed OLC mechanism can resynchronize bus frequencies with significantly improved transient performance.

A preliminary version has appeared in the Proceedings of the 3rd IEEE International Conference on Smart Grid Communications, Tainan City, Taiwan, November 2012.

I. INTRODUCTION

In power systems, regulation efforts traditionally focus on the generation side. For example, the automatic generation control adjusts the setpoints of generators based on area frequency deviations and unscheduled cross-area power flows [1]. To track the given setpoints at a faster time scale and improve stability, control mechanisms, such as the excitation system, speed governing system and power system stabilizer, are deployed on the generation side [2][3]. However, relying solely on generation control may not be enough. Due to limited ramping rate and large inertia, generators are suitable for minute-by-minute power balance, but may incur expensive wear-and-tear, high emissions, and low thermal efficiency when responding to regulation signals at intervals of seconds [4][5]. Complementary to generation control, we consider load control as an additional mechanism that provides fast and inexpensive power system regulation. Indeed the feasibility and efficiency of load control has already been demonstrated in several electricity markets. Long Island Power Authority (LIPA) developed LIPAE_{edge}, which provides 24.9 MW of demand reduction and 75 MW of spinning reserve by 23,400 loads [6]. Electric Reliability Council of Texas (ERCOT) has 50% of its 2400 MW reserve provided by loads. Pennsylvania-New Jersey-Maryland Interconnection (PJM) opens up the regulation market to participation by loads [4]. While most of the existing programs focus on direct manipulation of loads in a centralized scheme, the alternative strategy of decentralized load control via frequency measurement has also been studied in the literatures. Brooks *et al.* suggests that loads can sense and respond to frequency and provide regulation within 1 second [5]. Molina-Garcia *et al.* studies the aggregate response characteristics when individual loads are turned on/off as the frequency fluctuates [7]. Donnelly *et al.* develops proportional control of intelligent loads, and investigates the effect of distribution systems, the effect of discretized control, and the effect of time-delay of control actions, through the simulation of a 16-generator transmission network [8]. In our previous papers [9]–[11] we study a decentralized algorithm to minimize the cost of load control based on local frequency measurement and neighborhood communication. Frequency-based load control does not require communication to a centralized grid operator, and is thus suitable for large-scale decentralized deployment.

In this paper we consider a power transmission network where, at steady state, the generator frequencies at different buses (or in different balancing authorities) are synchronized to the

same nominal value and the mechanic power is balanced with the electric power at each bus. Suppose a small change in generation occurs on an arbitrary subset of the buses. How should the controllable loads in the network be reduced (or increased) in real time in a way that (i) balances the generation shortfall (or surplus), (ii) resynchronizes the bus frequencies, and (iii) minimizes a measure of aggregate cost of participation in such a load control? We formalize this question as an optimal load control (OLC) problem. The basic dynamics at each generation bus is described by swing equations that relate the imbalance between generation and load to the rate of frequency change. We assume the change in generation is small and the DC load flow model is reasonably accurate. We develop a frequency-based load control where loads are controlled based on locally measured frequency deviations and their individual cost functions. We prove that this frequency-based load control coupled with the system dynamics serve as a distributed primal-dual algorithm to solve OLC. Simulation of the IEEE 68-bus test system shows that the proposed OLC mechanism resynchronize bus frequencies with smaller steady-state error, smaller overshoot and shorter settling time, compared to the case with only local generator control mechanisms like power system stabilizers.

The paper is organized as follows. Section II describes a dynamic model of power networks and formulates OLC. Section III explains how the frequency-based load control and the system dynamics serve as a distributed primal-dual algorithm to solve OLC and its dual. Section IV provides the convergence analysis of the primal-dual algorithm. Section V illustrates the proposed scheme through the simulation of the IEEE 68-bus test system. Section VI concludes the paper. Section VII provides a detailed justification of our model of the branch power flow, both analytically and through simulation of the much more detailed dynamic model of power systems developed in [3][12].

II. PROBLEM FORMULATION

Let \mathbb{R} denote the set of real numbers and \mathbb{N} denote the set of non-zero natural numbers. For a set \mathcal{N} , let $|\mathcal{N}|$ denote its cardinality. A variable without a subscript usually denotes a vector with appropriate components, e.g., $\omega = (\omega_j, j \in \mathcal{N}) \in \mathbb{R}^{|\mathcal{N}|}$. For $a, b \in \mathbb{R}$, $a \leq b$, the expression $[\cdot]_a^b$ denotes $\max\{\min\{\cdot, b\}, a\}$. For a matrix A , let A^T denote its transpose. For a signal $\omega(t)$ of time, let $\dot{\omega}$ denote its time derivative $\frac{d\omega}{dt}$.

A. Transmission network model

The power transmission network is described by a graph $(\mathcal{N}, \mathcal{E})$ where $\mathcal{N} = \{1, \dots, |\mathcal{N}|\}$ is the set of buses and $\mathcal{E} \subseteq \mathcal{N} \times \mathcal{N}$ is the set of transmission lines connecting the buses. We make the following assumptions:¹

- The lines $(i, j) \in \mathcal{E}$ are lossless and characterized by their reactance x_{ij} .
- The voltage magnitudes $|V_j|$ of buses $j \in \mathcal{N}$ are constants.
- Reactive power injections at the buses and reactive power flows on the lines are ignored.

We assume that $(\mathcal{N}, \mathcal{E})$ is directed, with an arbitrary orientation, so that if $(i, j) \in \mathcal{E}$ then $(j, i) \notin \mathcal{E}$. We use (i, j) and $i \rightarrow j$ interchangeably to denote a link in \mathcal{E} , and use “ $i : i \rightarrow j$ ” and “ $k : j \rightarrow k$ ” respectively to denote the set of buses i that are predecessors of bus j and the set of buses k that are successors of bus j . We also assume without loss of generality that $(\mathcal{N}, \mathcal{E})$ is connected.

The network has two types of buses: generator buses and load buses. A generator bus not only has loads, but also an AC generator that converts mechanic power into electric power through a rotating prime mover. A load bus has only loads but no generator. We assume that the system is always under the three-phase balanced condition, and for a bus $j \in \mathcal{N}$, its phase a voltage at time t is $\sqrt{2}|V_j| \cos(\omega^0 t + \theta_j^0 + \Delta\theta_j(t))$, where ω^0 is the nominal frequency, θ_j^0 is the nominal phase angle, and $\Delta\theta_j(t)$ the time-varying phase angle deviation. The frequency at bus j is defined as $\omega_j := \omega^0 + \Delta\dot{\theta}_j$, and we call $\Delta\omega_j := \Delta\dot{\theta}_j$ the frequency deviation at bus j . We assume that the frequency deviations $\Delta\omega_j$ are small for all the buses $j \in \mathcal{N}$ and the differences $\Delta\theta_i - \Delta\theta_j$ between phase angle deviations are small across all the links $(i, j) \in \mathcal{E}$. We adopt a standard dynamic model, e.g., in [2, Section 11.4].

Generator buses. We assume coherency between the internal and terminal (bus) voltage phase angles of the generator so that these angles always differ by a constant even during the transient, which is discussed in more detail in Section VII-C. Then the dynamics on a generator bus j is modeled by the swing equation

$$M_j \Delta \dot{\omega}_j + D_j' \Delta \omega_j = P_j^{m'} - P_{loss,j}^0 - P_j^e,$$

¹These assumptions are similar to the standard DC approximation except that we do not assume the nominal phase angle difference is small across each link.

where $M_j > 0$ is the inertia constant of the generator. The term $D'_j \Delta\omega_j$ with $D'_j > 0$ represents the deviation in generator power loss due to friction, from its nominal value $P_{loss,j}^0$. Here $P_j^{m'}$ is the mechanic power injection to the generator, and P_j^e is the electric power export of the generator, which equals the sum of loads on bus j and the net power injection from bus j to the rest of the network.

In general, load power may depend on both the bus voltage magnitude (which is assumed fixed) and frequency. We distinguish between two types of loads, *frequency-sensitive* and *frequency-insensitive*. We assume frequency-sensitive (e.g., motor-type) loads increase linearly with frequency deviation and model the aggregate of these loads by $\hat{d}_j^0 + D''_j \Delta\omega_j$ with $D''_j > 0$, where \hat{d}_j^0 is its nominal power. We assume frequency-insensitive loads can be actively controlled and our goal is to design and analyze these control laws. Let d_j denote the aggregate of frequency-insensitive loads on bus j . Finally we allow constant power load P_j^l that is switched on or off. Then the electric power P_j^e is the sum of frequency-sensitive loads, frequency-insensitive loads, constant power load, and the net power injection from bus j to other buses:

$$P_j^e := \hat{d}_j^0 + D''_j \Delta\omega_j + d_j + P_j^l + \sum_{k:j \rightarrow k} P_{jk} - \sum_{i:i \rightarrow j} P_{ij}$$

where P_{jk} is the branch power flow from bus j to bus k .

Hence the dynamics on a generator bus j is

$$M_j \Delta \dot{\omega}_j = - (D_j \Delta\omega_j + d_j - P_j^m + P_j^{\text{out}} - P_j^{\text{in}})$$

where $D_j := D'_j + D''_j$, $P_j^m := P_j^{m'} - P_{j,loss}^0 - \hat{d}_j^0 - P_j^l$, and $P_j^{\text{out}} := \sum_{k:j \rightarrow k} P_{jk}$ and $P_j^{\text{in}} := \sum_{i:i \rightarrow j} P_{ij}$ are respectively the total branch power flows out and into bus j . Let $d_j^0, P_j^{m,0}, P_{ij}^0$ denote the nominal (operating) point at which $d_j^0 - P_j^{m,0} + P_j^{\text{out},0} - \Delta P_j^{\text{in},0} = 0$, and let $d_j(t) = d_j^0 + \Delta d_j(t)$, $P_j^m(t) = P_j^{m,0} + \Delta P_j^m(t)$, $P_{ij}(t) = P_{ij}^0 + \Delta P_{ij}(t)$. Then the deviations satisfy

$$M_j \Delta \dot{\omega}_j = - (D_j \Delta\omega_j + \Delta d_j - \Delta P_j^m + \Delta P_j^{\text{out}} - \Delta P_j^{\text{in}}). \quad (1)$$

Figure 1 is a schematic diagram of the generator bus model (1).

Load buses. For a load bus that has no generator, there is the following algebraic relation between the variables introduced above: ²

$$0 = D_j \Delta\omega_j + \Delta d_j - \Delta P_j^m + \Delta P_j^{\text{out}} - \Delta P_j^{\text{in}}. \quad (2)$$

²There may be load buses with large inertia that can be modeled by swing dynamics (1) as proposed in [13]. We will treat them as generator buses mathematically.

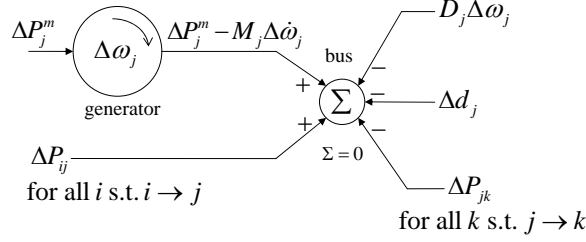


Fig. 1. Schematic diagram of a generator bus j , where $\Delta\omega_j$ is the frequency deviation; ΔP_j^m is the change in mechanic power; $D_j\Delta\omega_j$ characterizes the effect of generator friction and frequency-sensitive loads; Δd_j is the change in aggregate frequency-insensitive load; ΔP_{ij} is the deviation in branch power injected from another bus i to bus j ; ΔP_{jk} is the deviation in branch power delivered from bus j to another bus k .

Branch flows. The deviations ΔP_{ij} from the nominal branch flows follow the dynamics

$$\Delta \dot{P}_{ij} = B_{ij} (\Delta\omega_i - \Delta\omega_j), \quad (3)$$

where

$$B_{ij} := 3 \frac{|V_i||V_j|}{x_{ij}} \cos(\theta_i^0 - \theta_j^0) \quad (4)$$

is a constant related to nominal bus voltages and the line reactance. The same model was given in the literature, e.g., [1][2], based on the quasi-steady-state assumptions. However, we derive this model by solving the differential equation that characterizes the line induction to obtain three-phase instantaneous power flow, without explicitly using the quasi-steady-state assumptions. The detailed derivation is given in Section VII-A.

Dynamic network model. We denote the set of generator buses by \mathcal{G} , the set of load buses by \mathcal{L} , and use $|\mathcal{G}|$ and $|\mathcal{L}|$ to denote the number of generator buses and load buses, respectively. Without loss of generality, let $\mathcal{G} = \{1, \dots, |\mathcal{G}|\}$ and $\mathcal{L} = \{|\mathcal{G}| + 1, \dots, |\mathcal{N}|\}$. In summary, the dynamic model of the transmission network is specified by (1)–(3). To simplify notation, we drop the Δ from the variables denoting deviations and write (1)–(3) as

$$\dot{\omega}_j = -\frac{1}{M_j} (D_j \omega_j + d_j - P_j^m + P_j^{\text{out}} - P_j^{\text{in}}) \quad \text{for all } j \in \mathcal{G} \quad (5)$$

$$0 = D_j \omega_j + d_j - P_j^m + P_j^{\text{out}} - P_j^{\text{in}} \quad \text{for all } j \in \mathcal{L} \quad (6)$$

$$\dot{P}_{ij} = B_{ij} (\omega_i - \omega_j) \quad \text{for all } (i, j) \in \mathcal{E}, \quad (7)$$

where B_{ij} are given by (4). Hence for the rest of this paper all variables represent *deviations* from their nominal values. We will refer to the term $D_j\omega_j$ as the deviation in the (aggregate)

frequency-sensitive load even though it also includes the deviation in generator power loss due to friction. We will refer to the term P_j^m as the change in generation even though it may also include changes in constant power loads.

A steady state of the dynamic system described by (5)–(7) is defined as a state in which all power deviations and frequency deviations are constant over time, $\dot{\omega}_j = 0$ for $j \in \mathcal{G}$, and $\dot{P}_{ij} = 0$ for $(i, j) \in \mathcal{E}$.

Discussion. The model given by (5)–(7) captures the power system behavior at the timescale of seconds. In this paper we will only consider a step change in generation (constant deviations P_j^m), which implies that the proposed model does not include the action of turbine-governor (at a similar or slower timescale than the proposed model) that changes the mechanic power injection in response to frequency deviation to rebalance power. Nor does it include any secondary frequency control mechanism such as automatic generation control that operates at a much slower timescale to restore the nominal frequency. This model therefore explores the feasibility of the active control of frequency-insensitive loads at a fast timescale as a supplement to the turbine-governor mechanism to resynchronize frequency and rebalance power. Our results in Sections III and V suggest it is feasible.

The proposed model implicitly assumes that the time for individual frequencies ω_j to resynchronize (converge to a common system frequency, which may be time varying) after a power imbalance can be similar to the time for them to converge to their equilibrium value (which may be different from the nominal value). Whether this assumption holds depends on the electrical distances [14] between different buses. For buses that are close, they resynchronize almost instantly to a common frequency which then converges more slowly to the equilibrium value. For buses that are far away, their resynchronization times are similar to convergence times. These observations are shown by the simulation of a more realistic model; see Figure 9 in Section VII-C.

B. Optimal load control

Suppose a step change $P^m = (P_j^m, j \in \mathcal{N})$ in generation is injected to the set \mathcal{N} of buses. How should the frequency-insensitive loads $d = (d_j, j \in \mathcal{N})$ in the network be reduced (or increased) in real-time in a way that (i) balances the generation shortfall (or surplus), (ii) resynchronizes the bus frequencies, and (iii) minimizes a measure of aggregate disutility of participation in such

a load control? We now formalize these questions as an optimal load control (OLC) problem.

A change P^m in generation causes a nonzero frequency deviation ω_j at bus j . This frequency deviation incurs a cost to the aggregate frequency-sensitive load $\hat{d}_j := D_j \omega_j$ and suppose this cost is quadratic in frequency deviations, i.e., $\frac{1}{2D_j} \hat{d}_j^2 = \frac{1}{2} D_j \omega_j^2$ at bus j . Suppose the aggregate frequency-insensitive load at bus j is to be changed by an amount d_j and this change incurs a cost (disutility) of $c_j(d_j)$. We assume $-\infty < \underline{d}_j \leq d_j \leq \bar{d}_j < \infty$. Our goal is to minimize the total cost over d and \hat{d} while balancing generation and load across the network, written as

OLC:

$$\min_{\underline{d} \leq d \leq \bar{d}, \hat{d}} \sum_{j \in \mathcal{N}} \left(c_j(d_j) + \frac{1}{2D_j} \hat{d}_j^2 \right) \quad (8)$$

$$\text{subject to} \quad \sum_{j \in \mathcal{N}} (d_j + \hat{d}_j) = \sum_{j \in \mathcal{N}} P_j^m. \quad (9)$$

Remark 1. Note that (9) does not require the balance of generation and load at each individual bus, but only balance across the entire network. This constraint is less restrictive and offers more opportunity to minimize costs. Additional constraints can be imposed if it is desirable that certain buses balance their own supply and demand, e.g., for economic or regulatory reasons.

We assume the following condition throughout the paper:

Condition 1. The OLC problem is feasible, and the cost functions c_j are strictly convex and twice continuously differentiable on $[\underline{d}_j, \bar{d}_j]$.

Families of cost functions that satisfy Conditions 1 have been used in the literature [15][16]. The choice of cost functions can be based on physical characteristics of the loads and user comfort levels. Examples of particular cost functions can be found in [17] for air conditioners and in [18] for plug-in electric vehicles.

III. LOAD CONTROL AND SYSTEM DYNAMICS AS PRIMAL-DUAL ALGORITHM

We present the main results in this section, and prove them in Section IV.

A. Main results

The objective function of the dual problem of OLC is

$$\sum_{j \in \mathcal{N}} \Phi_j(\nu) := \sum_{j \in \mathcal{N}} \min_{\underline{d}_j \leq d_j \leq \bar{d}_j, \hat{d}_j} \left(c_j(d_j) - \nu d_j + \frac{1}{2D_j} \hat{d}_j^2 - \nu \hat{d}_j + \nu P_j^m \right),$$

where Φ_j can be written as

$$\Phi_j(\nu) := c_j(d_j(\nu)) - \nu d_j(\nu) - \frac{1}{2}D_j\nu^2 + \nu P_j^m \quad (10)$$

with

$$d_j(\nu) := \left[c_j'^{-1}(\nu) \right]_{\underline{d}_j}^{\bar{d}_j}. \quad (11)$$

This objective function has a scalar variable ν and is not separable across buses $j \in \mathcal{N}$. Its direct solution hence requires coordination across buses. We propose the following *distributed* version of the dual problem over the vector $\nu = (\nu_j, j \in \mathcal{N})$, where each bus j optimizes over its own variable ν_j which are constrained to be equal at optimality.

DOLC:

$$\begin{aligned} \max_{\nu} \quad & \Phi(\nu) := \sum_{j \in \mathcal{N}} \Phi_j(\nu_j) \\ \text{subject to} \quad & \nu_i = \nu_j \quad \text{for all } (i, j) \in \mathcal{E}. \end{aligned}$$

We have the following two lemmas regarding DOLC and its relation with OLC.

Lemma 1. The objective function Φ of DOLC is strictly concave over $\mathbb{R}^{|\mathcal{N}|}$.

Lemma 2. 1) DOLC has a unique optimal point ν^* with $\nu_i^* = \nu_j^* = \nu^*$ for all $i, j \in \mathcal{N}$.³
 2) OLC has a unique optimal point (d^*, \hat{d}^*) where $d_j^* = d_j(\nu^*)$ is given by (11) and $\hat{d}_j^* = D_j\nu^*$ for all $j \in \mathcal{N}$.

Lemma 1 and Lemma 2 are respectively proved in Sections VIII-A and VIII-B.

Instead of solving OLC directly, Lemma 2 suggests solving its dual DOLC and recovering the unique optimal point (d^*, \hat{d}^*) of the primal problem OLC from the unique dual optimal ν^* . To derive a distributed solution for DOLC, consider its Lagrangian

$$L(\nu, \pi) := \sum_{j \in \mathcal{N}} \Phi_j(\nu_j) - \sum_{(i, j) \in \mathcal{E}} \pi_{ij}(\nu_i - \nu_j), \quad (12)$$

where $\nu \in \mathbb{R}^{|\mathcal{N}|}$ is the (vector) variable for DOLC and $\pi \in \mathbb{R}^{|\mathcal{E}|}$ is the associated dual variable for the dual of DOLC. Hence π_{ij} , for all $(i, j) \in \mathcal{E}$, measure the cost of not synchronizing the

³For simplicity, we abuse the notation and use ν^* to denote both the vector $(\nu_j^*, j \in \mathcal{N})$ and the common value of its components. Its meaning should be clear given the context.

variables ν_i and ν_j across buses i and j . Using (10)–(12), a partial primal-dual algorithm for DOLC takes the form

$$\dot{\nu}_j = \gamma_j \frac{\partial L}{\partial \nu_j}(\nu, \pi) = -\gamma_j (d_j(\nu_j) + D_j \nu_j - P_j^m + \pi_j^{\text{out}} - \pi_j^{\text{in}}) \quad \text{for } j \in \mathcal{G} \quad (13)$$

$$0 = \frac{\partial L}{\partial \nu_j}(\nu, \pi) = - (d_j(\nu_j) + D_j \nu_j - P_j^m + \pi_j^{\text{out}} - \pi_j^{\text{in}}) \quad \text{for } j \in \mathcal{L} \quad (14)$$

$$\dot{\pi}_{ij} = -\xi_{ij} \frac{\partial L}{\partial \pi_{ij}}(\nu, \pi) = \xi_{ij}(\nu_i - \nu_j) \quad \text{for } (i, j) \in \mathcal{E}, \quad (15)$$

where $\gamma_j > 0$, $\xi_{ij} > 0$ are stepsizes and $\pi_j^{\text{out}} := \sum_{k:j \rightarrow k} \pi_{jk}$, $\pi_j^{\text{in}} := \sum_{i:i \rightarrow j} \pi_{ij}$. We interpret (13)–(15) as an algorithm iterating on the primal variables ν and dual variables π over time $t \geq 0$ as follows. For a generator bus j , given the current iterate $(\nu(t), \pi(t))$, one can use $\gamma_j \partial L(\nu(t), \pi(t)) / \partial \nu_j$ as the rate of change in ν_j . For a load bus j , the current iterate $\nu_j(t)$ is obtained as the solution of

$$\frac{\partial L}{\partial \nu_j}(\nu_j, \nu_{-j}(t), \pi(t)) = 0$$

given $\pi(t)$ and $\nu_{-j}(t) := (\nu_i(t), i \neq j)$. For a link $(i, j) \in \mathcal{E}$, given the current iterate $(\nu(t), \pi(t))$, one can use $-\xi_{ij} \partial L(\nu(t), \pi(t)) / \partial \pi_{ij}$ as the rate of change in π_{ij} .

In (13)–(15), the stepsizes γ_i and ξ_{ij} can take any positive values, and the initial values $(\nu(0), \pi(0))$ can also be taken arbitrarily. In particular, let

$$\gamma_j = M_j^{-1}, \quad \xi_{ij} = B_{ij},$$

and

$$\nu(0) = \omega(0), \quad \pi(0) = P(0),$$

where $\omega(0)$ and $P(0)$ are the frequency deviations and branch flow deviations at $t = 0$, the instant right after a step change P^m in generation has occurred. We use continuous time t as the iterating time in the primal-dual algorithm (13)–(15), and get a trajectory $(\nu(t), \pi(t))$ for $t \geq 0$. We compare it with $(\omega(t), P(t))$, the trajectory of frequency deviations and branch flow deviations, and find that the two trajectories take the same value for all t . Mathematically, (13)–(15) is identical to (5)–(7), if we identify ν with ω and π with P , and take $d_j = d_j(\omega_j)$ in (5)–(6).

For convenience, we collect here the system dynamics and load control:

$$\dot{\omega}_j = -\frac{1}{M_j} \left(d_j + \hat{d}_j - P_j^m + P_j^{\text{out}} - P_j^{\text{in}} \right) \quad \text{for } j \in \mathcal{G} \quad (16)$$

$$0 = d_j + \hat{d}_j - P_j^m + P_j^{\text{out}} - P_j^{\text{in}} \quad \text{for } j \in \mathcal{L} \quad (17)$$

$$\dot{P}_{ij} = B_{ij} (\omega_i - \omega_j) \quad \text{for } (i, j) \in \mathcal{E} \quad (18)$$

$$\hat{d}_j = D_j \omega_j \quad \text{for } j \in \mathcal{N} \quad (19)$$

$$d_j = \left[c_j'^{-1}(\omega_j) \right]_{\underline{d}_j}^{\bar{d}_j} \quad \text{for } j \in \mathcal{N}. \quad (20)$$

The dynamics (16)–(19) are automatically carried out by the power system while the active control (20) needs to be implemented at each frequency-insensitive load. Let $(d(t), \hat{d}(t), \omega(t), P(t))$ denote a trajectory of frequency-insensitive loads, frequency-sensitive loads, frequency deviations and branch flow deviations, generated by the dynamics (16)–(20) of the load-controlled system.

Theorem 1. Every trajectory $(d(t), \hat{d}(t), \omega(t), P(t))$ generated by (16)–(20) converges to a limit $(d^*, \hat{d}^*, \omega^*, P^*)$ as $t \rightarrow \infty$ such that

- 1) (d^*, \hat{d}^*) is the unique vector of optimal load control for OLC;
- 2) ω^* is the unique vector of optimal frequency deviations for DOLC;
- 3) P^* is a vector of optimal branch flows for the dual of DOLC.

We will prove Theorem 1 and other results in Section IV below.

B. Implications

Our main results have several important implications:

- 1) *Frequency-based load control:* The frequency-insensitive loads can be controlled using their individual marginal cost functions according to (20), based only on frequency deviations $\omega_j(t)$ (from their nominal values) that are measured at their local buses. Note that both the load control here and the generator droop control [1] respond to the difference between the nominal frequency and the actual frequency, but they are complementary. Load control is activated immediately after a sudden generation-load imbalance because many loads can respond quickly. Droop control is slower than load control due to larger time constants associated with valves and prime movers, but it compensates for a large amount of generation-load imbalance to prevent the frequency from wandering outside the desired

limit. Optimal load control explicitly uses cost functions of individual loads to share the required load reduction/increase optimally among all loads in the network, whereas in droop control generator outputs are adjusted proportionally to frequency deviations so that the sum of implicit cost functions which are quadratic in the changes of generator outputs is minimized.

- 2) *Complete decentralization.* The common operating frequency is a global signal that measures the power imbalance across the *entire* network. Our result implies that the local frequency deviation $\omega_j(t)$ at each bus turns out to convey exactly the right information about the global power imbalance for the loads themselves to make optimal decisions based on their own marginal cost functions. That is, with the right information, their local decisions turn out to be globally optimal. This result allows a completely decentralized solution without explicit communication among the buses.
- 3) *Reverse engineering of swing dynamics.* The frequency-based load control (20) coupled with the dynamics (16)–(19) of swing equations and branch power flows serve as a distributed primal-dual algorithm to solve OLC and its dual DOLC.
- 4) *Frequency and branch flows.* In the context of optimal load control, the frequency deviations $\omega_j(t)$ emerge as the Lagrange multipliers of OLC that measure the cost of power imbalance, whereas the branch flow deviations $P_{ij}(t)$ emerge as the Lagrange multipliers of DOLC that measure the cost of frequency asynchronism.
- 5) *Uniqueness of solution.* Lemma 2 implies that the optimal frequency ω^* is unique and hence the optimal load control (d^*, \hat{d}^*) is unique. As we show below, the optimal branch flows P^* are unique if and only if the network is a tree. Theorem 1 says nonetheless, that, even for mesh networks, any trajectory generated by the load control and system dynamics indeed converges to an optimal point, with the optimal value of P^* dependent on the initial condition right after a change in generation.
- 6) *Optimal frequency.* The structure of DOLC indicates that the frequencies at all the buses are synchronized at optimality even though they can be different during transient. However, the common frequency deviation ω^* at optimality is in general nonzero. This implies that while frequency-based load control and the swing dynamics can resynchronize bus frequencies to a unique common value after a change in generation, the new frequency may be different from the common operating frequency before the change. To respect the tight frequency

regulation limits in power systems, the new steady-state frequency deviation should be made small. Simulations in Section V show that the new steady-state frequency deviations are reasonably small with OLC. Other mechanisms, such as isochronous generators [1] or automatic generation control [2], will be needed to drive the new operating frequency to its nominal value, through, e.g., integral control of the frequency deviation.

Of course, many of these insights are well known; our results merely provide a fresh and unified interpretation within an optimization framework for frequency-based load control.

IV. CONVERGENCE ANALYSIS

This section is devoted to the proof of Theorem 1 and other properties as given by Theorems 2 – 3 below. Before going into the details, we first sketch out the key steps in establishing Theorem 1, the convergence of the trajectories generated by (16)–(20).

- 1) Theorem 2: The set of optimal points (ω^*, P^*) of DOLC and its dual and the set of equilibrium points of (16)–(20) are nonempty and the same. Denote both of them by Z^* .
- 2) Theorem 3: If $(\mathcal{N}, \mathcal{E})$ is a tree network, Z^* is a singleton with a unique equilibrium point (ω^*, P^*) , otherwise (if $(\mathcal{N}, \mathcal{E})$ is a mesh network), Z^* has an uncountably infinite number (a subspace) of equilibria with the same ω^* but different P^* .
- 3) Theorem 1: We use a Lyapunov-type technique to prove that every trajectory $(\omega(t), P(t))$ generated by (16)–(20) approaches a nonempty, compact subset Z^+ of Z^* as $t \rightarrow \infty$. Hence, if $(\mathcal{N}, \mathcal{E})$ is a tree network, it is straightforward from Theorem 3 that any trajectory $(\omega(t), P(t))$ converges to the unique optimal point (ω^*, P^*) . If $(\mathcal{N}, \mathcal{E})$ is a mesh network, we show with a more careful argument that $(\omega(t), P(t))$ still converges to a point in Z^+ , as opposed to wandering around Z^+ . Theorem 1 then follows from Lemma 2.

We now elaborate on these ideas.

Given ω , the optimal loads (d, \hat{d}) are uniquely determined by (19)–(20), hence we focus on the variables (ω, P) . Let C be the $|\mathcal{N}| \times |\mathcal{E}|$ incidence matrix with $C_{je} = 1$ if $e = (j, k) \in \mathcal{E}$ for some bus $k \in \mathcal{N}$, $C_{je} = -1$ if $e = (i, j) \in \mathcal{E}$ for some bus $i \in \mathcal{N}$, and $C_{je} = 0$ otherwise. Recall that we assumed that the first $|\mathcal{G}|$ buses $\{1, \dots, |\mathcal{G}|\}$ are generator buses and the remaining $|\mathcal{L}|$ buses $\{|\mathcal{G}| + 1, \dots, |\mathcal{N}|\}$ are load buses. Decompose C into an $|\mathcal{G}| \times |\mathcal{E}|$ submatrix $C_{\mathcal{G}}$ corresponding to generator buses and an $|\mathcal{L}| \times |\mathcal{E}|$ submatrix $C_{\mathcal{L}}$ corresponding to load buses, i.e., $C = \begin{bmatrix} C_{\mathcal{G}} \\ C_{\mathcal{L}} \end{bmatrix}$.

Similarly, let $\omega_{\mathcal{G}}$ and $\omega_{\mathcal{L}}$ respectively denote the vector of frequency deviations at generator buses and load buses, so $\omega^T = [\omega_{\mathcal{G}}^T \ \omega_{\mathcal{L}}^T]$. Let

$$\begin{aligned}\Phi_{\mathcal{G}}(\omega_{\mathcal{G}}) &:= \sum_{j \in \mathcal{G}} \Phi_j(\omega_j) \quad \text{and} \quad L_{\mathcal{G}}(\omega_{\mathcal{G}}, P) := \Phi_{\mathcal{G}}(\omega_{\mathcal{G}}) - \omega_{\mathcal{G}}^T C_{\mathcal{G}} P, \\ \Phi_{\mathcal{L}}(\omega_{\mathcal{L}}) &:= \sum_{j \in \mathcal{L}} \Phi_j(\omega_j) \quad \text{and} \quad L_{\mathcal{L}}(\omega_{\mathcal{L}}, P) := \Phi_{\mathcal{L}}(\omega_{\mathcal{L}}) - \omega_{\mathcal{L}}^T C_{\mathcal{L}} P.\end{aligned}$$

Identifying ν with ω and π with P , we can rewrite the Lagrangian for DOLC defined in (12), in terms of $\omega_{\mathcal{G}}$ and $\omega_{\mathcal{L}}$, as

$$L(\omega, P) = \Phi(\omega) - \omega^T C P = L_{\mathcal{G}}(\omega_{\mathcal{G}}, P) + L_{\mathcal{L}}(\omega_{\mathcal{L}}, P). \quad (21)$$

Then (16)–(20) (equivalently, (13)–(15)) can be rewritten in the vector form as

$$\dot{\omega}_{\mathcal{G}} = \Gamma_{\mathcal{G}} \left[\frac{\partial L_{\mathcal{G}}}{\partial \omega_{\mathcal{G}}}(\omega_{\mathcal{G}}, P) \right]^T = \Gamma_{\mathcal{G}} \left(\left[\frac{\partial \Phi_{\mathcal{G}}}{\partial \omega_{\mathcal{G}}}(\omega_{\mathcal{G}}) \right]^T - C_{\mathcal{G}} P \right) \quad (22)$$

$$0 = \frac{\partial L_{\mathcal{L}}}{\partial \omega_{\mathcal{L}}}(\omega_{\mathcal{L}}, P) = \left[\frac{\partial \Phi_{\mathcal{L}}}{\partial \omega_{\mathcal{L}}}(\omega_{\mathcal{L}}) \right]^T - C_{\mathcal{L}} P \quad (23)$$

$$\dot{P} = -\Xi \left[\frac{\partial L}{\partial P}(\omega, P) \right]^T = \Xi C^T \omega \quad (24)$$

where $\Gamma_{\mathcal{G}} := \text{diag}(\gamma_j, j \in \mathcal{G})$ and $\Xi := \text{diag}(\xi_{ij}, (i, j) \in \mathcal{E})$. The differential algebraic equations (22)–(24) describe the dynamics of the power network when active load control is performed.

A pair (ω^*, P^*) is called a *saddle point* of L if

$$L(\omega, P^*) \leq L(\omega^*, P^*) \leq L(\omega^*, P) \quad \text{for all } (\omega, P). \quad (25)$$

By [19, Section 5.4.2], (ω^*, P^*) is primal-dual optimal for DOLC and its dual if and only if it is a saddle point of $L(\omega, P)$. The following theorem establishes the equivalence between the primal-dual optimal points and the equilibrium points of (22)–(24).

Theorem 2. A point (ω^*, P^*) is primal-dual optimal for DOLC and its dual if and only if it is an equilibrium point of (22)–(24). Moreover, at least one primal-dual optimal point (ω^*, P^*) exists and ω^* is unique among all possible points (ω^*, P^*) that are primal-dual optimal.

Proof: Recall that we identified ν with ω and π with P . In DOLC, the objective function Φ is (strictly) concave over $\mathbb{R}^{|\mathcal{N}|}$ (by Lemma 1), its constraints are linear, and a finite optimal ω^* is attained (by Lemma 2). These facts imply that there is no duality gap between DOLC and its

dual, and there exists a dual optimal point P^* [19, Section 5.2.3]. Moreover, (ω^*, P^*) is optimal for DOLC and its dual if and only if the following Karush-Kuhn-Tucker (KKT) conditions [19, Section 5.5.3] are satisfied:

$$\text{Stationarity: } \frac{\partial \Phi}{\partial \omega}(\omega^*) = (CP^*)^T \quad (26)$$

$$\text{Primal feasibility: } \omega_i^* = \omega_j^* \quad \text{for all } (i, j) \in \mathcal{E}. \quad (27)$$

On the other hand, $(\omega^*, P^*) = (\omega_{\mathcal{G}}^*, \omega_{\mathcal{L}}^*, P^*)$ is an equilibrium point of (22)–(24) if and only if

$$\begin{aligned} \left[\frac{\partial \Phi_{\mathcal{G}}}{\partial \omega_{\mathcal{G}}}(\omega_{\mathcal{T}}^*) \right]^T &= C_{\mathcal{G}} P^* \\ \left[\frac{\partial \Phi_{\mathcal{L}}}{\partial \omega_{\mathcal{L}}}(\omega_{\mathcal{L}}^*) \right]^T &= C_{\mathcal{L}} P^* \\ \Xi C^T \omega^* &= 0, \end{aligned}$$

which are identical to (26)–(27). Hence, (ω^*, P^*) is primal-dual optimal if and only if it is an equilibrium point of (22)–(24). The uniqueness of ω^* is given by Lemma 2. \blacksquare

From Lemma 2, we denote the unique optimal point of DOLC by $\omega^* 1_{\mathcal{N}} = \begin{bmatrix} \omega^* 1_{\mathcal{G}} \\ \omega^* 1_{\mathcal{L}} \end{bmatrix}$, where $1_{\mathcal{N}} \in \mathbb{R}^{|\mathcal{N}|}$, $1_{\mathcal{G}} \in \mathbb{R}^{|\mathcal{G}|}$ and $1_{\mathcal{L}} \in \mathbb{R}^{|\mathcal{L}|}$ have all their elements equal to 1. From (26)–(27), define the nonempty set of equilibrium points of (22)–(24) (equivalently, primal-dual optimal points of DOLC and its dual) as

$$Z^* := \left\{ (\omega, P) \mid \omega = \omega^* 1_{\mathcal{N}}, CP = \left[\frac{\partial \Phi}{\partial \omega}(\omega^* 1_{\mathcal{N}}) \right]^T \right\}. \quad (28)$$

Let $(\omega^* 1_{\mathcal{N}}, P^*) = (\omega^* 1_{\mathcal{G}}, \omega^* 1_{\mathcal{L}}, P^*) \in Z^*$ be any equilibrium point of (22)–(24). We consider a candidate Lyapunov function

$$U(\omega, P) = \frac{1}{2} (\omega_{\mathcal{G}} - \omega^* 1_{\mathcal{G}})^T \Gamma_{\mathcal{G}}^{-1} (\omega_{\mathcal{G}} - \omega^* 1_{\mathcal{G}}) + \frac{1}{2} (P - P^*)^T \Xi^{-1} (P - P^*). \quad (29)$$

Obviously $U(\omega, P) \geq 0$ for all (ω, P) with equality if and only if $\omega_{\mathcal{G}} = \omega^* 1_{\mathcal{G}}$ and $P = P^*$. We will show below that $\dot{U}(\omega, P) \leq 0$ for all (ω, P) , where \dot{U} denotes the derivative of U along the trajectory $(\omega(t), P(t))$.

Even though U depends explicitly only on $\omega_{\mathcal{G}}$ and P , \dot{U} depends on $\omega_{\mathcal{L}}$ as well through (24). However, it will prove convenient to express \dot{U} as a function of only $\omega_{\mathcal{G}}$ and P . To this end, write (23) as $F(\omega_{\mathcal{L}}, P) = 0$. Then $\frac{\partial F}{\partial \omega_{\mathcal{L}}}(\omega_{\mathcal{L}}, P) = \frac{\partial^2 \Phi_{\mathcal{L}}}{\partial \omega_{\mathcal{L}}^2}(\omega_{\mathcal{L}})$ is nonsingular for all $(\omega_{\mathcal{L}}, P)$ from the

proof of Lemma 1 in Section VIII-A. By the inverse function theorem [20], $\omega_{\mathcal{L}}$ can be written as a continuously differentiable function of P , denoted by $\omega_{\mathcal{L}}(P)$, with

$$\frac{\partial \omega_{\mathcal{L}}}{\partial P}(P) = \left(\frac{\partial^2 \Phi_{\mathcal{L}}}{\partial \omega_{\mathcal{L}}^2}(\omega_{\mathcal{L}}(P)) \right)^{-1} C_{\mathcal{L}}. \quad (30)$$

Then we can rewrite the Lagrangian $L(\omega, P)$ as a function of only $(\omega_{\mathcal{G}}, P)$ as

$$L(\omega, P) = L_{\mathcal{G}}(\omega_{\mathcal{G}}, P) + L_{\mathcal{L}}(\omega_{\mathcal{L}}(P), P) = \tilde{L}(\omega_{\mathcal{G}}, P). \quad (31)$$

We have the following lemma, proved in VIII-C, regarding the properties of \tilde{L} .

Lemma 3. \tilde{L} is strictly concave in $\omega_{\mathcal{G}}$ and convex in P .

Rewrite (22)–(24) as

$$\dot{\omega}_{\mathcal{G}} = \Gamma_{\mathcal{G}} \left[\frac{\partial \tilde{L}}{\partial \omega_{\mathcal{G}}}(\omega_{\mathcal{G}}, P) \right]^T \quad (32)$$

$$\dot{P} = -\Xi \left[\frac{\partial \tilde{L}}{\partial P}(\omega_{\mathcal{G}}, P) \right]^T. \quad (33)$$

Then the derivative of U along any trajectory $(\omega(t), P(t))$ generated by (22)–(24) is

$$\begin{aligned} \dot{U}(\omega, P) &= (\omega_{\mathcal{G}} - \omega^* 1_{\mathcal{G}})^T \Gamma_{\mathcal{G}}^{-1} \dot{\omega}_{\mathcal{G}} + (P - P^*)^T \Xi^{-1} \dot{P} \\ &= \frac{\partial \tilde{L}}{\partial \omega_{\mathcal{G}}}(\omega_{\mathcal{G}}, P) (\omega_{\mathcal{G}} - \omega^* 1_{\mathcal{G}}) - \frac{\partial \tilde{L}}{\partial P}(\omega_{\mathcal{G}}, P) (P - P^*) \end{aligned} \quad (34)$$

$$\leq \tilde{L}(\omega_{\mathcal{G}}, P) - \tilde{L}(\omega^* 1_{\mathcal{G}}, P) + \tilde{L}(\omega_{\mathcal{G}}, P^*) - \tilde{L}(\omega_{\mathcal{G}}, P) \quad (35)$$

$$= L(\omega_{\mathcal{G}}, \omega^* 1_{\mathcal{L}}, P^*) - \tilde{L}(\omega^* 1_{\mathcal{G}}, P) \quad (36)$$

$$\leq L(\omega^* 1_{\mathcal{N}}, P) - \tilde{L}(\omega^* 1_{\mathcal{G}}, P) \quad (37)$$

$$\begin{aligned} &= L_{\mathcal{G}}(\omega^* 1_{\mathcal{G}}, P) + L_{\mathcal{L}}(\omega^* 1_{\mathcal{L}}, P) - [L_{\mathcal{G}}(\omega^* 1_{\mathcal{G}}, P) + L_{\mathcal{L}}(\omega_{\mathcal{L}}(P), P)] \\ &\leq 0. \end{aligned} \quad (38)$$

Here (34) follows from (32)–(33). The inequality in (35) results from Lemma 3. The equality in (36) holds since $\omega_{\mathcal{L}}(P^*) = \omega^* 1_{\mathcal{L}}$ by (26). The inequality in (37) is due to $L(\omega_{\mathcal{G}}, \omega^* 1_{\mathcal{L}}, P^*) \leq L(\omega^* 1_{\mathcal{N}}, P^*) \leq L(\omega^* 1_{\mathcal{N}}, P)$ by the saddle point condition (25). The inequality in (38) follows since $\omega_{\mathcal{L}}(P)$ is the maximizer of $L_{\mathcal{L}}(\cdot, P)$ given P , by the concavity of $L_{\mathcal{L}}$ in $\omega_{\mathcal{L}}$ and the definition of $\omega_{\mathcal{L}}(P)$.

The next lemma, proved in Section VIII-D, characterizes the set in which the value of U does not change over time.

Lemma 4. $\dot{U}(\omega, P) = 0$ if and only if either of the following two conditions holds.

1)

$$\omega_{\mathcal{G}} = \omega^* 1_{\mathcal{G}} \quad \text{and} \quad C_{\mathcal{L}} P = \left[\frac{\partial \Phi_{\mathcal{L}}}{\partial \omega_{\mathcal{L}}} (\omega^* 1_{\mathcal{L}}) \right]^T. \quad (39)$$

2)

$$\omega_{\mathcal{G}} = \omega^* 1_{\mathcal{G}} \quad \text{and} \quad \omega_{\mathcal{L}}(P) = \omega^* 1_{\mathcal{L}}. \quad (40)$$

Lemma 4 motivates the definition of the set

$$E := \{(\omega, P) \mid \dot{U}(\omega, P) = 0\} = \left\{ (\omega, P) \mid \omega = \omega^* 1_{\mathcal{N}}, C_{\mathcal{L}} P = \left[\frac{\partial \Phi_{\mathcal{L}}}{\partial \omega_{\mathcal{L}}} (\omega^* 1_{\mathcal{L}}) \right]^T \right\} \quad (41)$$

in which $\dot{U} = 0$ along any trajectory $(\omega(t), P(t))$. The definition of Z^* in (28) implies that $Z^* \subseteq E$, as shown in Figure 2. As shown in the figure, E may contain points that are not in Z^* .

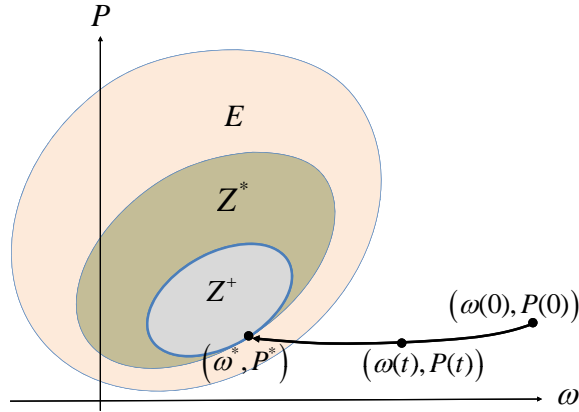


Fig. 2. E is the set on which $\dot{U} = 0$, Z^* is the set of equilibrium points of (22)–(24), and Z^+ is a compact subset of Z^* to which all solutions $(\omega(t), P(t))$ approach as $t \rightarrow \infty$. Indeed, every solution $(\omega(t), P(t))$ converges to a point $(\omega^*, P^*) \in Z^+$ that is dependent on the initial state.

Nonetheless, every accumulation point (limit point of any convergent sequence sampled from the trajectory) of a solution $(\omega(t), P(t))$ of (22)–(24) is in Z^* , as the next lemma shows.

Lemma 5. Every solution $(\omega(t), P(t))$ of (22)–(24) approaches a nonempty, compact subset (denoted Z^+) of Z^* as $t \rightarrow \infty$.

The proof of Lemma 5 is given in Section VIII-E. The sets $Z^+ \subseteq Z^* \subseteq E$ are illustrated in Figure 2. Lemma 5 only guarantees that $(\omega(t), P(t))$ approaches Z^+ as $t \rightarrow \infty$, but does not guarantee that it converges to any point in Z^* . We now show that $(\omega(t), P(t))$ indeed converges to an equilibrium point in Z^+ . Indeed, the convergence is immediate in the special simple case when Z^* is a singleton, but needs a more careful argument when Z^* has multiple points. The next theorem reveals the relation between the number of points in Z^* and the network topology.

Theorem 3. 1) Suppose $(\mathcal{N}, \mathcal{E})$ is a tree, then Z^* is a singleton.

2) Suppose $(\mathcal{N}, \mathcal{E})$ is a mesh (i.e., contains a cycle if regarded as an undirected graph), then Z^* has an uncountably infinite number of points with the same ω^* but different P^* .

Proof: Recall that any point $(\omega^*, P^*) \in Z^*$ is a solution of (26)–(27). Let $h^* := CP^* = \left[\frac{\partial \Phi}{\partial \omega}(\omega^*)\right]^T$. Let \tilde{C} be the $(|\mathcal{N}| - 1) \times |\mathcal{E}|$ reduced incidence matrix obtained from C by removing any one of its rows. Then \tilde{C} has a full row rank of $|\mathcal{N}| - 1$ [21]. Consider the corresponding equation

$$\tilde{C}P^* = \tilde{h}^* \quad (42)$$

where \tilde{h}^* is obtained from h^* by removing the corresponding row. Since ω^* is unique, so is \tilde{h}^* . If $(\mathcal{N}, \mathcal{E})$ is a tree, then $|\mathcal{E}| = |\mathcal{N}| - 1$. Hence \tilde{C} is square and invertible, so P^* is unique. If $(\mathcal{N}, \mathcal{E})$ is a (connected) mesh, then $|\mathcal{E}| > |\mathcal{N}| - 1$, so \tilde{C} has a nontrivial null space and there are uncountably many P^* that solves (42). ■

With all the results above, we can now finish the proof of Theorem 1.

Proof of Theorem 1: For the case in which $(\mathcal{N}, \mathcal{E})$ is a tree, Lemma 5 and Theorem 3(1) guarantees that every trajectory $(\omega(t), P(t))$ converges to the unique primal-dual optimal point (ω^*, P^*) of DOLC and its dual, which, by Lemma 2, immediately implies Theorem 1.

For the case in which $(\mathcal{N}, \mathcal{E})$ is a mesh, since $\dot{U}(\omega, P) \leq 0$ for all (ω, P) , any solution $(\omega(t), P(t))$ for $t \geq 0$ stays in the compact set $\{(\omega, P) | U(\omega, P) \leq U(\omega(0), P(0))\}$. Hence there exists a convergent subsequence $\{(\omega(t_k), P(t_k)), k \in \mathbb{N}\}$, where $0 \leq t_1 < t_2 < \dots$ and $t_k \rightarrow \infty$ as $k \rightarrow \infty$, such that $\lim_{k \rightarrow \infty} \omega(t_k) = \omega^\infty$ and $\lim_{k \rightarrow \infty} P(t_k) = P^\infty$ for some $(\omega^\infty, P^\infty)$. Lemma 5 implies that $(\omega^\infty, P^\infty) \in Z^+ \subseteq Z^*$, and hence $\omega^\infty = \omega^* 1_{\mathcal{N}}$ by (28). Recall that the Lyapunov function U in (29) can be defined in terms of any equilibrium point $(\omega^*, P^*) \in Z^*$. In particular,

select $(\omega^*, P^*) = (\omega^\infty, P^\infty)$, i.e.,

$$U(\omega, P) := \frac{1}{2} (\omega_{\mathcal{G}} - \omega^* \mathbf{1}_{\mathcal{G}})^T \Gamma_{\mathcal{G}}^{-1} (\omega_{\mathcal{G}} - \omega^* \mathbf{1}_{\mathcal{G}}) + \frac{1}{2} (P - P^\infty)^T \Xi^{-1} (P - P^\infty).$$

Since $U \geq 0$ and $\dot{U} \leq 0$ along all trajectories $(\omega(t), P(t))$, $U(\omega(t), P(t))$ must converge as $t \rightarrow \infty$. Moreover it converges to 0 due to the continuity of U in both ω and P :

$$\lim_{t \rightarrow \infty} U(\omega(t), P(t)) = \lim_{k \rightarrow \infty} U(\omega(t_k), P(t_k)) = U(\omega^\infty, P^\infty) = 0.$$

The equation above implies that the trajectory $(\omega(t), P(t))$ converges to $(\omega^\infty, P^\infty) \in Z^+ \subseteq Z^*$, a primal-dual optimal point for DOLC and its dual. Theorem 1 then follows from Lemma 2. ■

Remark 2. The standard technique of using a Lyapunov function that is quadratic in primal-dual variables was first proposed by Arrow *et al.* [22], and has been revisited many times, e.g., in [23] [24]. We apply a variation of this general technique to our particular problem and extend the results in the literature. First, with the algebraic equation (23) in the system, we take a Lyapunov function candidate that is quadratic in part of the primal variables $\omega_{\mathcal{G}}$ and the dual variables P , and show that it is indeed a Lyapunov function. Second, in the case when there are a subspace of equilibrium points due to the non-tree topology of the network, we show that the system trajectory converges to one of the equilibrium points instead of oscillating around the equilibrium set, without any modifications to the primal-dual algorithm like those in [24].

V. CASE STUDIES

In this section, we illustrate the performance of OLC through simulation of the IEEE 68-bus New England/New York interconnection test system [3]. The single line diagram of the 68-bus system is given in Figure 3. We run the simulation on Power System Toolbox [12], with two-axis subtransient reactance generator model, IEEE type DC1 exciter model, classical power system stabilizer (PSS) model, and AC power flow model on non-zero resistance lines. The detailed models and their parameters can be found in the data file and manual of the toolbox.

In the system, there are 35 load buses serving different types of loads, including constant active current loads, constant impedance loads, and induction motor loads, with a total real power of 18.23 GW. In addition, we add three loads to buses 1, 7 and 27, each making a step increase of real power by 1 pu (based on 100 MVA), as the change P_j^m in generation. We also select 30 load buses, each having a load that is actively controlled based on OLC. In the simulation,

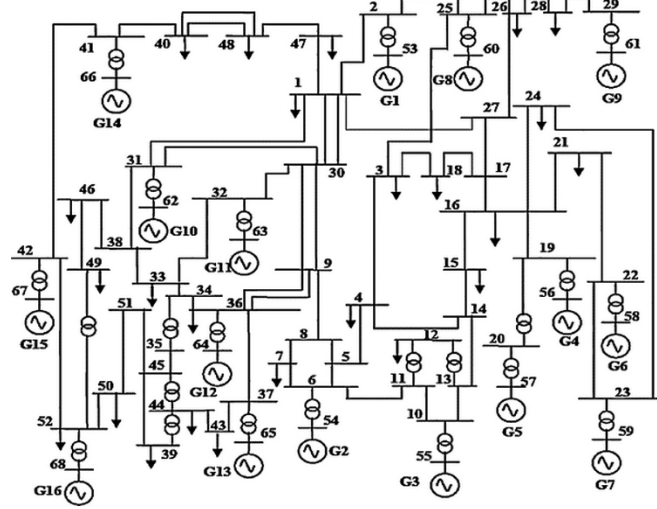


Fig. 3. Single line diagram of the 68-bus New England/New York test system.

we take the same bounds $[d, \bar{d}]$ with $\underline{d} = -\bar{d}$ for each of the 30 controllable loads, and call the value of $30 \times \bar{d}$ the *total size of controllable loads*. We will show simulation results with different sizes of controllable loads below. In the simulation, the cost function of a controllable load d_j is defined as $c_j(d_j) = d_j^2/(2\alpha)$, with the same α over all the loads. As an example, we select $\alpha = 100$ pu. To incorporate some practical consideration, the loads are not controlled continuously over time. Instead, they measure local frequencies and control their power every 250 ms, which takes a relatively conservative estimate for the rate of load control [25].

Since we have theoretically proved that OLC drives the system to a steady state where the cost of load control is minimized and total generation and total load are balanced, in the simulation we mainly focus on the transient performance, specifically, how the frequency and voltage change after a change in generation. We also look at how effective OLC is as a complement to the existing control mechanisms, such as the power system stabilizer (PSS), by enabling/disabling the PSS module in the simulation toolbox. Figures 4(a) and 4(b) respectively show the frequency and voltage at bus 66, under four cases: (i) no PSS, no OLC; (ii) with PSS, no OLC; (iii) no PSS, with OLC; and (iv) with PSS and OLC. In both cases (ii) and (iv), we take the total size of controllable loads as 1.5 pu. We observe that whether PSS is used or not, adding OLC can always improve the transient performance of frequency, in the sense that both the overshoot and the settling time (defined as the time after which the difference between the frequency and

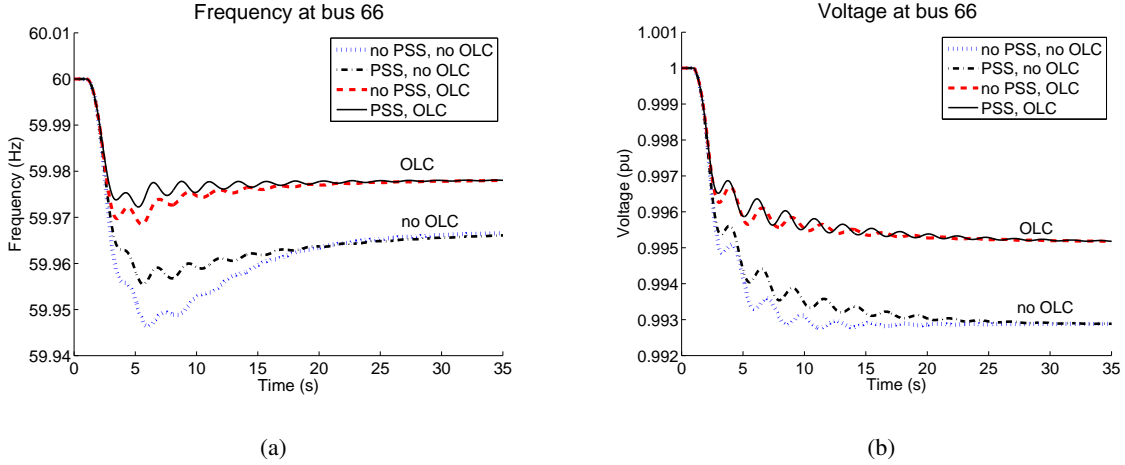


Fig. 4. The (a) frequency and (b) voltage at bus 66, under four cases: (i) no PSS, no OLC; (ii) with PSS, no OLC; (iii) no PSS, with OLC; (iv) with PSS and OLC.

its new steady-state value never goes beyond 5% of the difference between its old and new steady-state values) are decreased. Using OLC also leads to a smaller steady-state frequency error. Comparison between cases (ii) and (iii) also suggests that using OLC solely without PSS produces a much better performance than using PSS solely without OLC. However the improvement of the transient performance of voltage is not as significant as frequency, which may be due to the fact that voltage depends more on reactive power injections while here OLC does not control the reactive power of loads. The effect of reactive load control to support voltage will be investigated in future work.

To better quantify the performance improvement due to OLC we plot in Figures 5(a) – 5(c) the new steady-state value, the lowest value (which indicates overshoot) and the settling time of frequency at bus 66, against total size of controllable loads, as shown . Here PSS is always enabled. We observe that using OLC always leads to a higher new steady-state frequency (a smaller steady-state error), a higher lowest frequency (a smaller overshoot), and a shorter settling time, regardless of the total size of controllable loads. As the total size of controllable loads increases, the steady-state error and overshoot decrease almost linearly until a saturation around 1.5 pu. There is a similar trend for the settling time, though the linear dependence is only approximate. In summary, OLC improves both the steady-state value and the transient performance of frequency, and, in general, deploying more and larger controllable loads enables

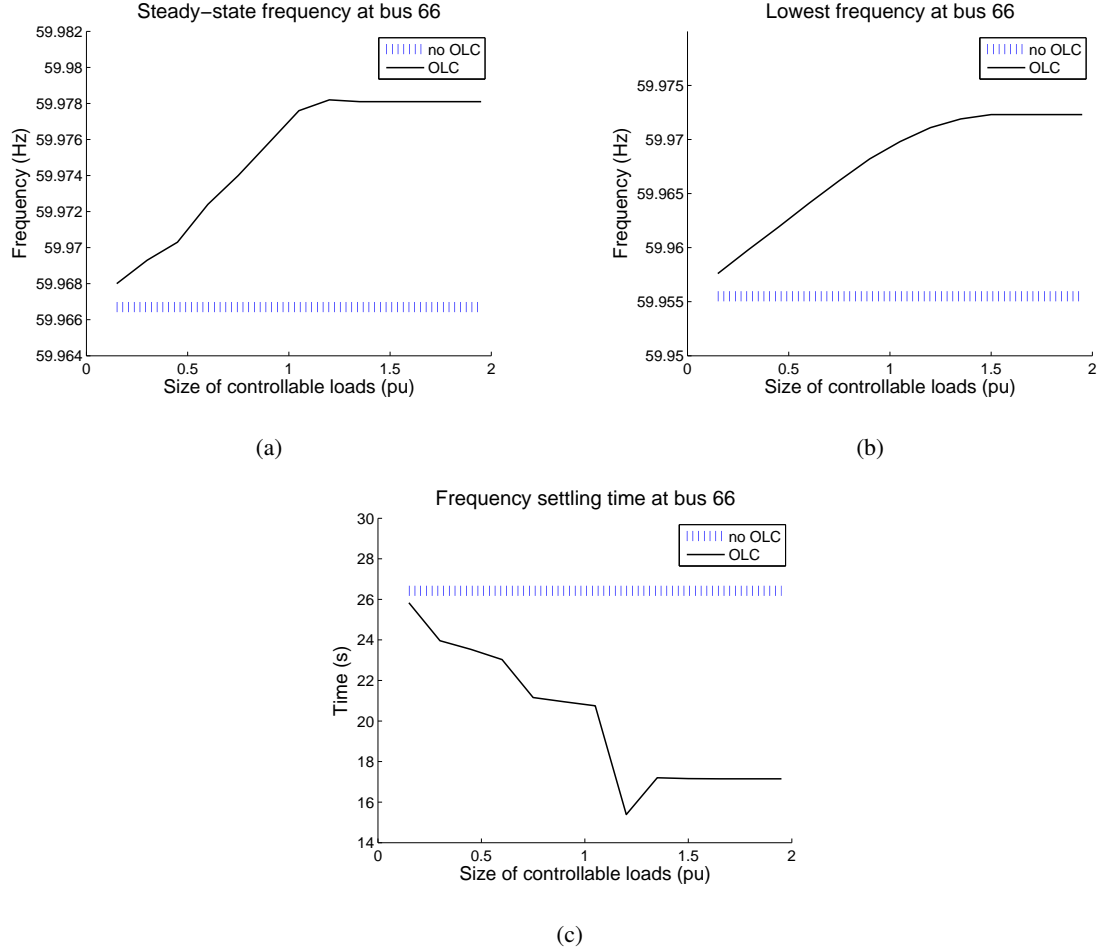


Fig. 5. The (a) new steady-state value, (b) lowest value and (c) settling time of frequency at bus 66, against the total size of controllable loads.

larger improvement.

VI. CONCLUSION

We have formulated an optimal load control (OLC) problem in power transmission networks where the objective is to minimize the cost of participation in load control subject to power balance across the network. We have shown that the dynamics of the swing equations and the branch power flows, coupled with a frequency-based load control, serve as a distributed primal-dual algorithm to solve the dual problem of OLC. Even though the system has multiple equilibrium points (nonunique branch power flows), we have proved that it nonetheless converges to an optimal point. Simulation of the IEEE 68-bus test system confirmed that the proposed

mechanism can resynchronize bus frequencies with significantly improved transient performance compared to using only local generator control mechanisms.

ACKNOWLEDGMENT

We thank Ross Baldick, Janusz Bialek, Jeremy Lin, Lang Tong, and Felix Wu for very helpful discussions on our dynamic network model. We also thank Lijun Chen for discussions on our approach and Alec Brooks of AeroVironment for suggestions on practical issues. This work is supported by NSF NetSE grant CNS 0911041, ARPA-E grant de-ar0000226, Southern California Edison, National Science Council of Taiwan R.O.C. grant NSC 101-3113-P-008-001, NSF CNS Award 1312390, the Caltech Resnick Institute, and the Okawa Foundation.

VII. APPENDIX: MODELING DETAILS

In this section, we first derive the branch flow dynamic model given by (3)–(4). Then, to show the accuracy of the model introduced in Section II-A (referred to as “the analytic model”), we use a more realistic simulation model developed in [3][12] (the same one we used in Section V) as a benchmark and demonstrate that the analytic model is a reasonable approximation of the simulation model. The key conclusions from simulations are summarized as follows:

- 1) The internal and terminal voltage phase angles of the generator swing coherently, i.e., the rotating speed of a generator is always the same as the frequency at the generator bus.
- 2) Different buses may have their own frequencies and buses that are far apart in electrical distance resynchronize at a similar timescale as the convergence time.
- 3) The simulation model and the analytic model exhibit similar transient behaviors and steady state values of bus frequencies and branch power flows.

A. Derivation of the branch flow model

We assume that the system is always under the three-phase balanced condition, the frequency deviations $\Delta\omega_j$ are small, and the differences $\Delta\theta_i - \Delta\theta_j$ between phase angle deviations are small across all the links $(i, j) \in \mathcal{E}$. Specifically, $\Delta\omega_j$ is negligible compared to ω^0 , and an approximation of a quantity to the first order of $\Delta\theta_i - \Delta\theta_j$ is reasonable. Now we show that the deviations ΔP_{ij} in three-phase instantaneous power flows from their nominal values follow the dynamics in (3)–(4), by solving the differential equation that characterizes the line induction.

Without loss of generality suppose that buses i and j are wye-connected [2] and each of the three lines has the same inductance L and zero resistance. Let the phase a voltages at buses i and j at time t be $v_i^a(t) = \sqrt{2}|V_i| \cos(\omega^0 t + \theta_i^0 + \Delta\theta_i(t))$ and $v_j^a(t) = \sqrt{2}|V_j| \cos(\omega^0 t + \theta_j^0 + \Delta\theta_j(t))$ respectively, and assume the voltage magnitudes are fixed. Denote the phase a current from i to j at time t by $i_{ij}^a(t)$.

For $t \leq 0$, suppose $\Delta\theta_j(t) = 0$ for all the buses j . Hence the system is at a steady state with $i_{ij}^a(t) = \sqrt{2}|I_0| \cos(\omega^0 t + \theta_c^0)$. From phasor calculations we have

$$|I_0| = \frac{|V_0|}{x_{ij}}$$

$$\theta_c^0 = \tan^{-1} \left[\frac{|V_j| \cos \theta_j^0 - |V_i| \cos \theta_i^0}{|V_i| \sin \theta_i^0 - |V_j| \sin \theta_j^0} \right]$$

where $x_{ij} := \omega^0 L$, and $|V_0| := \sqrt{|V_i|^2 + |V_j|^2 - 2|V_i||V_j| \cos(\theta_i^0 - \theta_j^0)}$. Then, we have

$$i_{ij}^a(0) = \sqrt{2}|I_0| \cos \theta_c^0 = \frac{\sqrt{2} (|V_i| \sin \theta_i^0 - |V_j| \sin \theta_j^0)}{x_{ij}}. \quad (43)$$

For $t \geq 0$, we have

$$L \frac{di_{ij}^a}{dt} = v_i^a - v_j^a,$$

whose solution is

$$\begin{aligned} i_{ij}^a(t) &= i_{ij}^a(0) + \frac{1}{L} \int_0^t (v_i^a(\tau) - v_j^a(\tau)) d\tau \\ &\approx i_{ij}^a(0) + \frac{\sqrt{2}}{\omega^0 L} [|V_i| \sin(\omega^0 t + \theta_i^0 + \Delta\theta_i(t)) - |V_i| \sin \theta_i^0] \\ &\quad - \frac{\sqrt{2}}{\omega^0 L} [|V_j| \sin(\omega^0 t + \theta_j^0 + \Delta\theta_j(t)) - |V_j| \sin \theta_j^0] \\ &= \frac{\sqrt{2}}{x_{ij}} [|V_i| \sin(\omega^0 t + \theta_i^0 + \Delta\theta_i(t)) - |V_j| \sin(\omega^0 t + \theta_j^0 + \Delta\theta_j(t))], \end{aligned} \quad (44)$$

where the approximate equality is due to the assumption that $\Delta\dot{\theta}_j = \Delta\omega_j$ are negligible compared to ω^0 , and the last equality is due to (43).

From (44) the instantaneous real power injection from i to j at phase a is

$$\begin{aligned}
p_{ij}^a &= v_i^a v_{ij}^a \\
&= 2 \frac{|V_i|^2}{x_{ij}} \sin(\omega^0 t + \theta_i^0 + \Delta\theta_i) \cos(\omega^0 t + \theta_i^0 + \Delta\theta_i) \\
&\quad - 2 \frac{|V_i||V_j|}{x_{ij}} \sin(\omega^0 t + \theta_j^0 + \Delta\theta_j) \cos(\omega^0 t + \theta_i^0 + \Delta\theta_i) \\
&= \frac{|V_i|^2}{x_{ij}} \sin(2\omega^0 t + 2\theta_i^0 + 2\Delta\theta_i) + \frac{|V_i||V_j|}{x_{ij}} \sin(\theta_i^0 - \theta_j^0 + \Delta\theta_i - \Delta\theta_j) \\
&\quad - \frac{|V_i||V_j|}{x_{ij}} \sin(2\omega^0 t + \theta_i^0 + \theta_j^0 + \Delta\theta_i + \Delta\theta_j).
\end{aligned} \tag{45}$$

Since we assumed the system is under the three-phase balanced condition, replacing θ_i^0 and θ_j^0 in (45) with $\theta_i^0 - \frac{2}{3}\pi$ and $\theta_j^0 - \frac{2}{3}\pi$, we get p_{ij}^b ; replacing θ_i^0 and θ_j^0 in (45) with $\theta_i^0 + \frac{2}{3}\pi$ and $\theta_j^0 + \frac{2}{3}\pi$, we get p_{ij}^c . Hence the three-phase instantaneous real power flow is (to the first order of $\Delta\theta_i - \Delta\theta_j$)

$$\begin{aligned}
P_{ij} &= p_{ij}^a + p_{ij}^b + p_{ij}^c = 3 \frac{|V_i||V_j|}{x_{ij}} \sin(\theta_i^0 - \theta_j^0 + \Delta\theta_i - \Delta\theta_j) \\
&\approx P_{ij}^0 + \Delta P_{ij}
\end{aligned} \tag{46}$$

where

$$P_{ij}^0 = 3 \frac{|V_i||V_j|}{x_{ij}} \sin(\theta_i^0 - \theta_j^0)$$

is the nominal branch power flow, and

$$\Delta P_{ij} = 3 \frac{|V_i||V_j|}{x_{ij}} \cos(\theta_i^0 - \theta_j^0) (\Delta\theta_i - \Delta\theta_j)$$

is the deviation in branch power flow. By $\Delta\omega_i = \Delta\dot{\theta}_i, \Delta\omega_j = \Delta\dot{\theta}_j$, we get the branch flow dynamics in (3)–(4).

B. Power flow behavior

In Sections VII-B, VII-C, and VII-D, we first simulate the IEEE 68-bus test system to a steady state (called “pre-change steady state”) and then introduce the same step change in generation as in Section V. Then we compare the post-change behavior of the simulation with prediction of the analytic model introduced in Section II-A.

We first check the branch flow dynamic model (3)–(4), which was derived above. Repeat it here as

$$\Delta \dot{P}_{ij} = B_{ij}(\Delta\omega_i - \Delta\omega_j) \quad \text{for } (i, j) \in \mathcal{E} \quad (47)$$

where $B_{ij} = 3|V_i||V_j|\cos(\theta_i^0 - \theta_j^0)/x_{ij}$ is a constant under the assumption of constant voltage magnitudes and zero line resistances. We use the pre-change steady-state voltage magnitudes $|V_i|$, $|V_j|$ and angles θ_i^0 , θ_j^0 from the simulation to determine B_{ij} . Post change, we substitute the frequency deviations $\Delta\omega_i(t)$ from the simulation into (47) to compute the trajectory $P_{ij}(t)$ that would result if $\Delta \dot{P}_{ij}$ is indeed proportional to the frequency difference, and compare it with the $P_{ij}(t)$ trajectory from the simulation. Since the simulation model is more detailed than the analytic model (1)–(2) for generator and load buses, using $\Delta\omega_i(t)$ from the simulation to calculate $P_{ij}(t)$ isolates the behavior of branch flow modeled by (47).

The results are shown in Figures 6(a)–6(e) on five lines. The simulation model and the model given by (47) exhibit similar transient behaviors and steady state values, suggesting that (47) is a reasonable approximation of the simulation model.

Specifically, to quantitative the accuracy of steady state, define the steady-state error as

$$\text{steady-state error} := \frac{|f_{\text{modeled}} - f_{\text{simulated}}|}{|f_{\text{simulated}}|} \times 100\%,$$

where “steady-state” refers to the post-change steady state, f_{modeled} refers to the steady-state frequency predicted by (47), and $f_{\text{simulated}}$ refers to the steady-state frequency given by the simulation. Figure 7 shows the errors on 84 of the 86 lines in the test system. Of these 84 lines, all errors are within 11% and most within 2%.

The two lines whose errors are not included in Figure 7 are the following:

- 1) Line from buses 1 to 2: simulated power flow is -0.1105 pu; modeled power flow is -0.0836 pu; steady-state error is 24.35%. However the effect of the change in generation at steady state is similar between the simulation and the model prediction: the difference between pre-change steady state and the post-change steady state is 0.7258 pu in simulation and 0.7527 pu from the model, yielding an error of 3.71%.
- 2) Line from buses 52 to 42: simulated power flow is -0.0068 pu; modeled power flow is 0.0198 pu; steady-state error is 393%. Note that the steady-state values themselves are much smaller than the average value (about 5pu). Moreover the difference between the

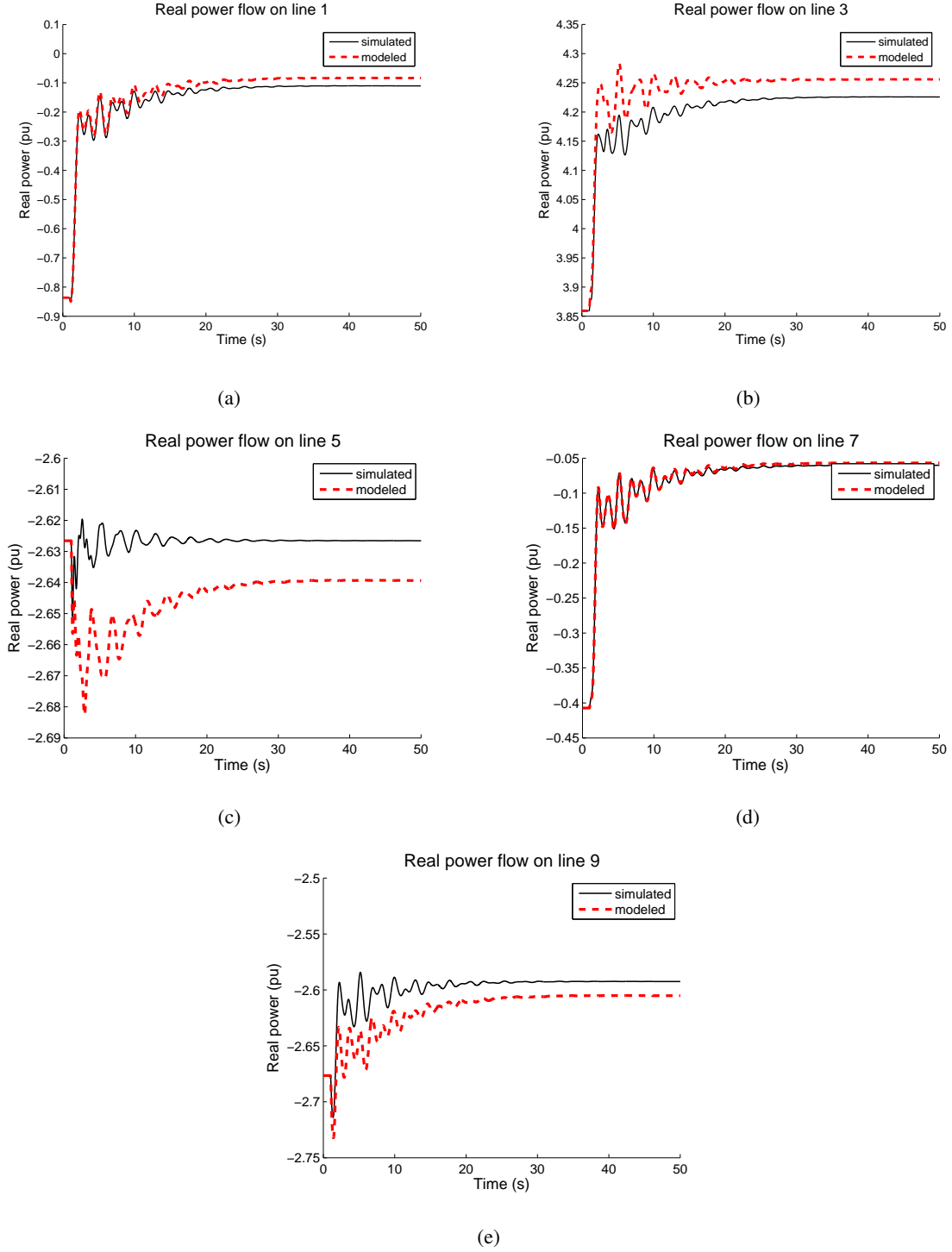


Fig. 6. Real power flows on five of the lines in the 68-bus test system, both given by the simulation (“simulated” in the legend) and given by the model $\Delta \dot{P}_{ij} = B_{ij}(\Delta \omega_i - \Delta \omega_j)$ (“modeled” in the legend).

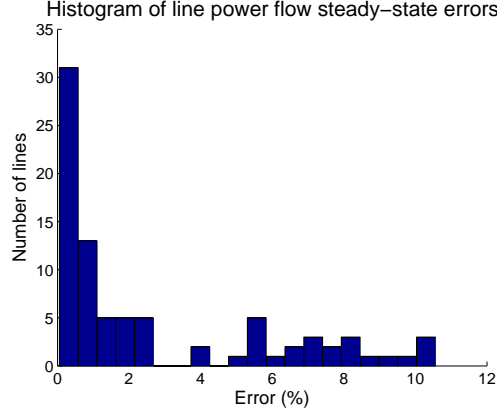


Fig. 7. Histogram of steady-state real power flow errors (between the values given by simulation and predicted by the analytic model) on 84 out of the 86 lines in the IEEE 68-bus test system.

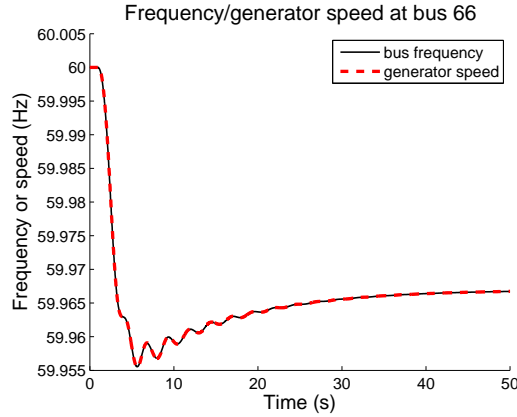


Fig. 8. Bus frequency is the same as the generator speed at bus 66 of the IEEE 68-bus test system.

pre-change steady state and the post-change steady state is 0.950 pu in simulation and 0.1215 pu from the model, yielding an error of 27.98%.

C. Frequency behavior

We check the assumption made in Section II-A that the internal and terminal voltage phase angles of the generator always differ by a constant, i.e., the rotating speed of a generator is always the same as the frequency at the generator bus. As an example, Figure 8 shows both the bus frequency and the generator speed at bus 66 in the IEEE 68-bus test system, which supports this assumption.

We then check a key modeling assumption that different buses may have their own frequencies and buses that are far apart in electrical distance resynchronize at a similar timescale as the convergence time. To this end we divide the 68 buses into the following 4 groups, with buses in each group being close in electrical distance to each other:

- 1) Group 1 has buses 41, 42, 66, 67, 52, and 68;
- 2) Group 2 has buses 2, 3, 4, 5, 6, 7, 8, 10, 11, 12, 13, 14, 15, 16, 17, 18, 19, 20, 21, 22, 23, 24, 25, 26, 27, 28, 29, 53, 54, 55, 56, 57, 58, 59, 60, and 61;
- 3) Group 3 has buses 1, 9, 30, 31, 32, 33, 34, 35, 36, 37, 38, 39, 40, 43, 44, 45, 46, 47, 48, 49, 51, 62, 63, 64, and 65;
- 4) Group 4 has bus 50 only.

Figure 9 shows all 68 bus frequencies from the simulation, in four groups. We see that the frequencies at different buses within the same group are almost identical even during transient, but the bus frequencies of different groups are different during transient. Moreover the time it takes for these different frequencies to converge to a common system frequency is on the same order as the time for these frequencies to reach their (common) equilibrium value.

D. Accuracy of the analytic model

To show the accuracy of the analytic model (1)–(4), we model the 68-bus test system as a 4-node network, where each node represents an area (group of buses shown in Figure 9) within which all buses have roughly the same frequency. Of these 4 nodes, we model nodes 1–3 as generator nodes with positive inertia by the swing dynamics (1), and model node 4 (which has bus 50 only) as a load node with zero inertia by the algebraic equation (2).

Figure 10 shows the frequencies at four of the 68 buses, which are representatives for the four groups, both given by the simulation and given by the analytic model. Figure 11 shows the real power flows on two of the lines connecting two groups, both given by the simulation and given by the analytic model. As we can see, the analytic model is a reasonable approximation of the more realistic simulation model.

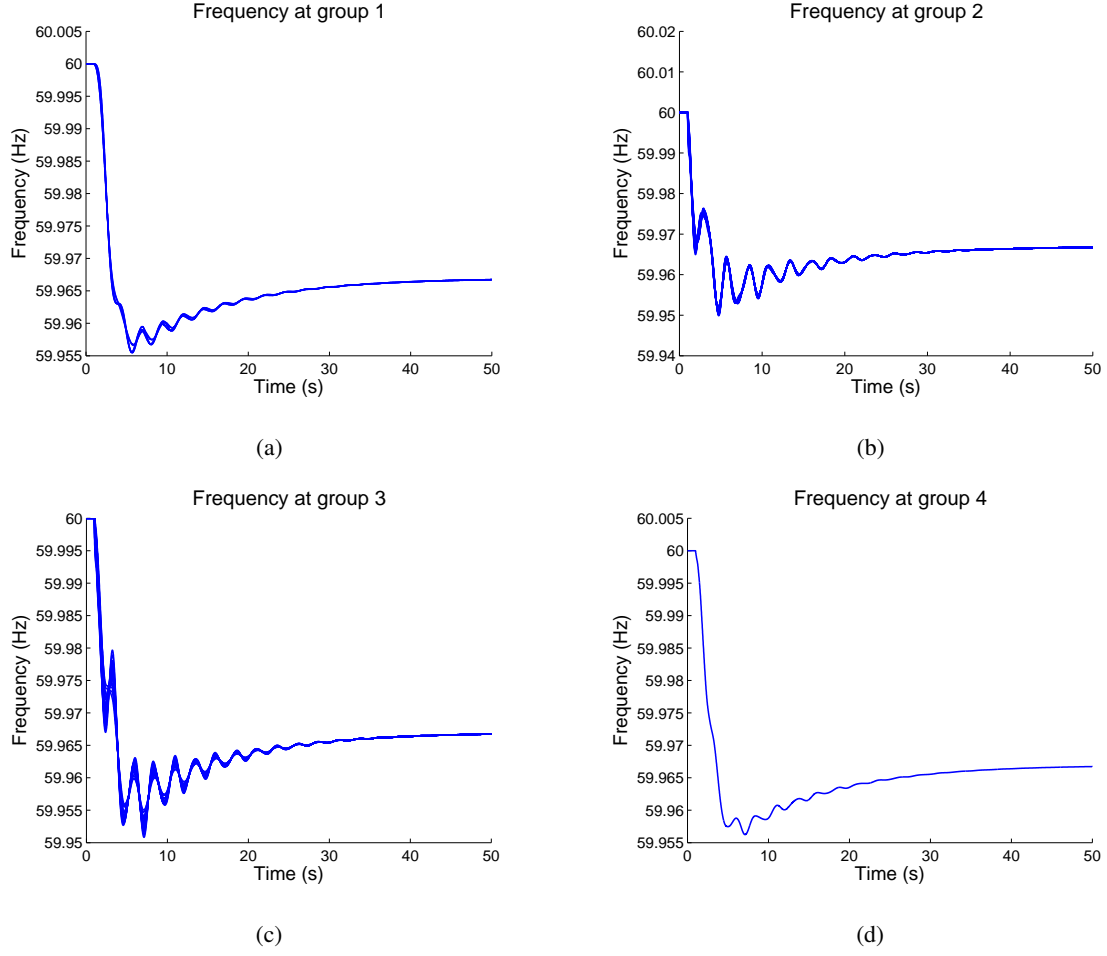


Fig. 9. Bus frequencies in each of the four groups.

VIII. APPENDIX: PROOFS

A. Proof of Lemma 1

From (11), either $c'_j(d_j(\nu)) = \nu$ or $d'_j(\nu) = 0$. Hence, in (10) we have

$$\frac{d}{d\nu} (c_j(d_j(\nu)) - \nu d_j(\nu)) = c'_j(d_j(\nu))d'_j(\nu) - d_j(\nu) - \nu d'_j(\nu) = -d_j(\nu),$$

and thus

$$\frac{\partial \Phi}{\partial \nu_j}(\nu) = \Phi'_j(\nu_j) = -d_j(\nu_j) - D_j \nu_j + P_j^m.$$

Hence the Hessian of Φ is diagonal. Moreover, since $d_j(\nu_j)$ given by (11) is nondecreasing in ν_j , we have

$$\frac{\partial^2 \Phi}{\partial \nu_j^2}(\nu) = \Phi''_j(\nu_j) = -d'_j(\nu_j) - D_j < 0.$$

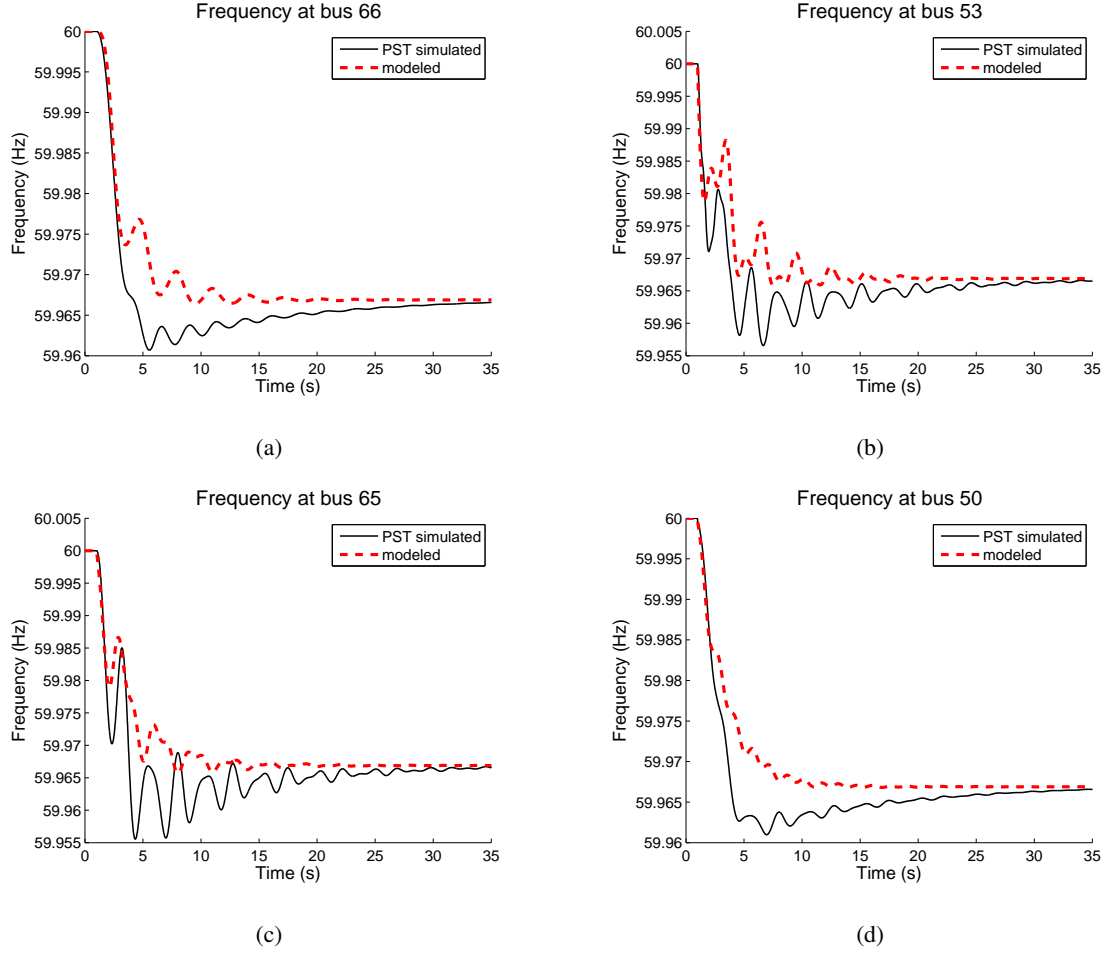


Fig. 10. Frequencies at four buses which are the representatives for the four groups, both given by the simulation (“PST simulated” in the legend) and given by the analytic model (“modeled” in the legend).

Hence Φ is strictly concave over $\mathbb{R}^{|\mathcal{N}|}$. □

B. Proof of Lemma 2

Let g denote the objective function of OLC with the domain $\mathcal{D} := [\underline{d}_1, \bar{d}_1] \times \cdots \times [\underline{d}_{|\mathcal{N}|}, \bar{d}_{|\mathcal{N}|}] \times \mathbb{R}^{|\mathcal{N}|}$. Since c_j is continuous on $[\underline{d}_j, \bar{d}_j]$, $\sum_j c_j(d_j)$ is lower bounded, i.e., $\sum_j c_j(d_j) > \underline{C}$ for some $\underline{C} > -\infty$. Let (d', \hat{d}') be a feasible point of OLC (which exists by Condition 1). Define the set $\mathcal{D}' := \left\{ (d, \hat{d}) \in \mathcal{D} \mid \hat{d}_j^2 \leq 2D_j(g(d', \hat{d}') - \underline{C}) \text{ for all } j \in \mathcal{N} \right\}$. Note that for any $(d, \hat{d}) \in \mathcal{D} \setminus \mathcal{D}'$, there is some $i \in \mathcal{N}$ such that $\hat{d}_i^2 > 2D_i(g(d', \hat{d}') - \underline{C})$, thus

$$g(d, \hat{d}) > \underline{C} + \frac{\hat{d}_i^2}{2D_i} > g(d', \hat{d}').$$

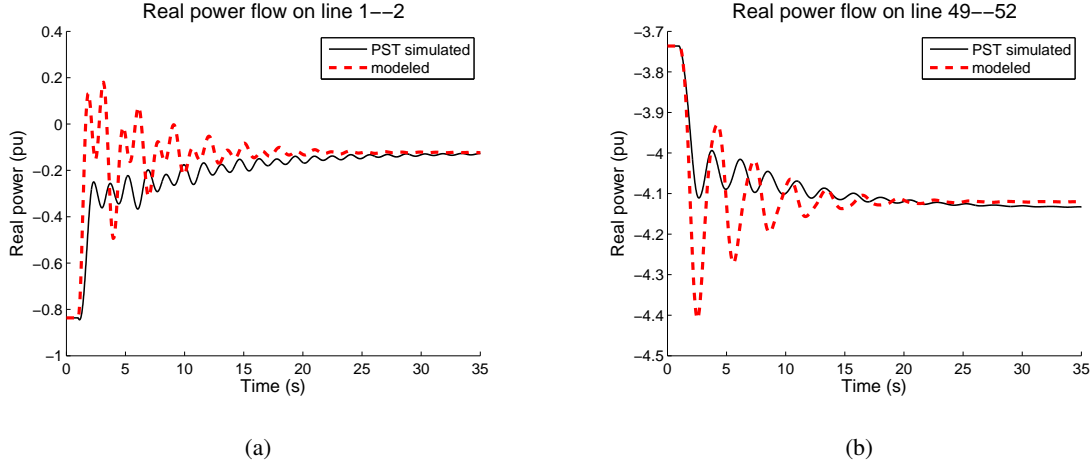


Fig. 11. Real power flows on two lines which connect two different areas, both given by the simulation (“PST simulated” in the legend) and given by the analytic model (“modeled” in the legend).

Hence, any optimal point of OLC must lie in \mathcal{D}' . By Condition 1, the objective function g of OLC is continuous and strictly convex over the compact, convex set \mathcal{D}' , thus it has a minimum $g^* > -\infty$ attained at a unique point $(d^*, \hat{d}^*) \in \mathcal{D}'$.

Note that OLC has a feasible point $(d, \hat{d}) \in \text{relint } \mathcal{D}$, where $\text{relint } \mathcal{D}$ denotes the relative interior of \mathcal{D} [19]. Indeed, let $(d', \hat{d}') \in \mathcal{D}$ be a feasible point of OLC, then we can obtain (d, \hat{d}) by letting $d_j = (\underline{d}_j + \bar{d}_j) / 2$, $\hat{d}_j = \hat{d}'_j - d_j + d'_j$. Also note that the only constraint of OLC is affine. Hence, there is zero duality gap between OLC and its dual, and a dual optimal ν^* is attained since $g^* > -\infty$ [19, Section 5.2.3]. By Section VIII-A, $\sum_{j \in \mathcal{N}} \Phi_j''(\nu) = -\sum_{j \in \mathcal{N}} (d'_j(\nu) + D_j) < 0$, i.e., the objective function of the dual problem of OLC is strictly concave over \mathbb{R} , which implies the uniqueness of ν^* . Moreover, by the definition of dual problem, the optimal point (d^*, \hat{d}^*) of OLC should satisfy $d_j^* = d_j(\nu^*)$ given by (11) and $\hat{d}_j^* = D_j \nu^*$ for all $j \in \mathcal{N}$. \square

C. Proof of Lemma 3

From the proof of Lemma 1, the Hessian $\frac{\partial^2 \tilde{L}}{\partial \omega_{\mathcal{G}}^2}(\omega_{\mathcal{G}}, P) = \frac{\partial^2 \Phi_{\mathcal{G}}}{\partial \omega_{\mathcal{G}}^2}(\omega_{\mathcal{G}})$ is diagonal and negative definite for all $\omega_{\mathcal{G}} \in \mathbb{R}^{|\mathcal{G}|}$. Therefore \tilde{L} is strictly concave in $\omega_{\mathcal{G}}$. Moreover, from (31) and the fact that $\frac{\partial \tilde{L}}{\partial \omega_{\mathcal{L}}}(\omega_{\mathcal{L}}(P), P) = 0$, we have

$$\frac{\partial \tilde{L}}{\partial P}(\omega_{\mathcal{G}}, P) = -\omega_{\mathcal{G}}^T C_{\mathcal{G}} - \omega_{\mathcal{L}}^T(P) C_{\mathcal{L}}. \quad (48)$$

Therefore we have (using (30))

$$\frac{\partial^2 \tilde{L}}{\partial P^2}(\omega_{\mathcal{G}}, P) = -C_{\mathcal{L}}^T \frac{\partial \omega_{\mathcal{L}}}{\partial P}(P) = -C_{\mathcal{L}}^T \left(\frac{\partial^2 \Phi_{\mathcal{L}}}{\partial \omega_{\mathcal{L}}^2}(\omega_{\mathcal{L}}(P)) \right)^{-1} C_{\mathcal{L}}.$$

From the proof of Lemma 1, $\frac{\partial^2 \Phi_{\mathcal{L}}}{\partial \omega_{\mathcal{L}}^2}$ is diagonal and negative definite. Hence $\frac{\partial^2 \tilde{L}}{\partial P^2}(\omega_{\mathcal{G}}, P)$ is positive semidefinite and \tilde{L} is convex in P (\tilde{L} may not be strictly convex in P because $C_{\mathcal{L}}$ is not necessarily of full rank). \square

D. Proof of Lemma 4

The equivalence of (40) and (39) follows directly from the definition of $\omega_{\mathcal{L}}(P)$. To prove that (40) is necessary and sufficient for $\dot{U}(\omega, P) = 0$, we first claim that the discussion preceding the lemma implies that $(\omega, P) = (\omega_{\mathcal{G}}, \omega_{\mathcal{L}}, P)$ satisfies $\dot{U}(\omega, P) = 0$ if and only if

$$\omega_{\mathcal{G}} = \omega^* 1_{\mathcal{G}} \quad \text{and} \quad \frac{\partial \tilde{L}}{\partial P}(\omega_{\mathcal{G}}, P) (P - P^*) = 0. \quad (49)$$

Indeed, if (49) holds, then the expression in (34) evaluates to zero. Conversely, if $\dot{U}(\omega, P) = 0$, then the inequality in (35) must hold with equality, which is possible only if $\omega_{\mathcal{G}} = \omega^* 1_{\mathcal{G}}$ since \tilde{L} is *strictly* concave in $\omega_{\mathcal{G}}$. Then we must have $\frac{\partial \tilde{L}}{\partial P}(\omega_{\mathcal{G}}, P) (P - P^*) = 0$ since the expression in (34) needs to be zero. Hence we only need to establish the equivalence of (49) and (40). Indeed, with $\omega_{\mathcal{G}} = \omega^* 1_{\mathcal{G}}$, the other part of (49) becomes

$$\frac{\partial \tilde{L}}{\partial P}(\omega^* 1_{\mathcal{G}}, P) (P - P^*) = -[\omega^* 1_{\mathcal{G}}^T \quad \omega_{\mathcal{L}}^T(P)] C(P - P^*) \quad (50)$$

$$= -[0 \quad \omega_{\mathcal{L}}^T(P) - \omega^* 1_{\mathcal{L}}^T] C(P - P^*) \quad (51)$$

$$= -(\omega_{\mathcal{L}}(P) - \omega^* 1_{\mathcal{L}})^T C_{\mathcal{L}}(P - P^*) \\ = -(\omega_{\mathcal{L}}(P) - \omega^* 1_{\mathcal{L}})^T \left[\frac{\partial \Phi_{\mathcal{L}}}{\partial \omega_{\mathcal{L}}}(\omega_{\mathcal{L}}(P)) - \frac{\partial \Phi_{\mathcal{L}}}{\partial \omega_{\mathcal{L}}}(\omega^* 1_{\mathcal{L}}) \right]^T, \quad (52)$$

where (50) follows from (48), (51) follows from $1_{\mathcal{N}}^T C = 0$, and (52) follows from (23) and (26). Note that $\Phi_{\mathcal{L}}$ is separable over ω_j for $j \in \mathcal{L}$ and, from (10), $\Phi'_j(\omega_j) = -d_j(\omega_j) - D_j \omega_j + P_j^m$. Writing $D_{\mathcal{L}} := \text{diag}(D_j, j \in \mathcal{L})$, we hence have

$$\frac{\partial \tilde{L}}{\partial P}(\omega^* 1_{\mathcal{G}}, P) (P - P^*) = (\omega_{\mathcal{L}}(P) - \omega^* 1_{\mathcal{L}})^T D_{\mathcal{L}} (\omega_{\mathcal{L}}(P) - \omega^* 1_{\mathcal{L}}) \\ + \sum_{j \in \mathcal{L}} (\omega_j(P) - \omega^*) (d_j(\omega_j(P)) - d_j(\omega^*)). \quad (53)$$

Since $d_j(\omega_j)$ given by (11) is nondecreasing in ω_j , each term in the summation above is nonnegative for all P . Hence (53) evaluates to zero if and only if $\omega_{\mathcal{L}}(P) = \omega^* 1_{\mathcal{L}}$, establishing the equivalence of (49) and (40). \square

E. Proof of Lemma 5

The proof of LaSalle's invariance principle in [26, Theorem 3.4] shows that $(\omega(t), P(t))$ approaches its positive limit set Z^+ which is nonempty, compact, invariant, and a subset of E , as $t \rightarrow \infty$. It is sufficient to show that $Z^+ \subseteq Z^*$, i.e., considering any point $(\omega, P) = (\omega_G, \omega_L, P) \in Z^+$, to show that $(\omega, P) \in Z^*$. By (28), (41) and the fact that $(\omega, P) \in E$, we only need to show that

$$C_G P = \left[\frac{\partial \Phi_G}{\partial \omega_G}(\omega_G) \right]^T. \quad (54)$$

Since Z^+ is invariant with respect to (22)–(24), a trajectory $(\omega(t), P(t))$ that starts in Z^+ must stay in Z^+ , and hence stay in E . By (41), $\omega_G(t) = \omega^* 1_G$ for all $t \geq 0$, and therefore $\dot{\omega}_G(t) = 0$ for all $t \geq 0$. Hence, by (22), any trajectory $(\omega(t), P(t))$ in Z^+ should satisfy

$$C_G P(t) = \left[\frac{\partial \Phi_G}{\partial \omega_G}(\omega_G(t)) \right]^T$$

for all $t \geq 0$, which implies that (54) holds for any $(\omega, P) \in Z^+$. \square

REFERENCES

- [1] A. J. Wood and B. F. Wollenberg, *Power Generation, Operation, and Control*, 2nd Edition. NJ: John Wiley & Sons, Inc., 1996.
- [2] A. R. Bergen and V. Vittal, *Power Systems Analysis*, 2nd ed. Upper Saddle River, NJ: Prentice Hall, 2000.
- [3] G. Rogers. *Power System Oscillations*. MA, US: Kluwer Academic Publishers, 2000.
- [4] G. Heffner, C. Goldman, B. Kirby and M. Kintner-Meyer, "Loads providing ancillary services: Review of international experience," *Technical Report, Lawrence Berkeley National Laboratory*, LBNL-62701, May 2007.
- [5] A. Brooks, E. Liu, D. Reicher, C. Spirakis and B. Wehl, "Demand dispatch: Using real-time control of demand to help balance generation and load," *IEEE Power&Energy Magazine*, vol. 8, no. 3, pp. 21-30, 2010.
- [6] B. Kirby, "Spinning Reserve From Responsive Loads," *Technical Report, Oak Ridge National Laboratory*, ORNL/TM-2003/19, March 2003.
- [7] A. Molina-Garcia, F. Bouffard and D. S. Kirschen, "Decentralized demand-side contribution to primary frequency control," *IEEE Transactions on Power Systems*, vol. 26, no. 1, pp. 411-419, 2001.
- [8] M. Donnelly, D. Harvey, R. Munson and D. Trudnowski, "Frequency and stability control using decentralized intelligent loads: Benefits and pitfalls," in *Proc. of the IEEE Power and Energy Society General Meeting*, Minneapolis, MN, USA, 2010.
- [9] C. Zhao, U. Topcu, S. Low, "Frequency-based load control in power systems," in *Proc. of American Control Conference*, Montreal, Quebec, Canada, June 2012.
- [10] C. Zhao, U. Topcu, S. Low, "Fast load control with stochastic frequency measurement," in *Proc. of the IEEE Power and Energy Society General Meeting*, San Diego, CA, USA, July 2012.

- [11] C. Zhao, U. Topcu, S. Low, "Optimal load control via frequency measurement and neighborhood area communication," *IEEE Transactions on Power Systems*, 2013.
- [12] J. Chow and G. Rogers, *Power System Toolbox*, Version 3.0, 1991-2008.
- [13] M. D. Ilic, L. Xie, U. A. Khan, J. M. F. Moura, "Modeling of future cyberphysical energy systems for distributed sensing and control," *IEEE Transactions on Systems, Man, and Cybernetics – Part A: Systems and Humans*, vol. 40, no. 4, pp. 825-838, 2010.
- [14] M. Ilic and Q. Liu, "Toward sensing, communications and control architectures for frequency regulation in systems with highly variable resources," *Control and Optimization Theory for Electric Smart Grids*. New York: Springer, 2012.
- [15] M. Fahrioglu, F. L. Alvarado, "Designing incentive compatible contracts for effective demand management," *IEEE Transactions on Power Systems*, vol. 15, no. 4, pp. 1255-1260, 2000.
- [16] P. Samadi, A. Mohsenian-Rad, R. Schober, V. W. S. Wong, J. Jatskevich, "Optimal Real-time pricing algorithm based on utility maximization for smart grid," *Proc. of the IEEE SmartGridComm*, Brussels, Belgium, October 2011.
- [17] B. Ramanathan, V. Vittal, "A framework for evaluation of advanced direct load control with minimum disruption," *IEEE Transactions on Power Systems*, vol. 23, no. 4, pp. 1681-1688, 2008.
- [18] Z. Ma, D. Callaway, I. Hiskens, "Decentralized charging control for large populations of plug-in vehicles: application of the Nash certainty equivalence principle," *Proc. of IEEE Multi-Conference on Systems and Control*, Yokohama, Japan, September 2010.
- [19] S. Boyd and L. Vandenberghe, *Convex Optimization*, UK: Cambridge University Press, 2004.
- [20] W. Rudin, *Principles of Mathematical Analysis*, 3rd ed. New York: McGraw-Hill Book Co., 1976. pp.
- [21] P. V. Mieghem, *Graph Spectra for Complex Networks*. UK: Cambridge University Press, 2011.
- [22] K. Arrow, L. Hurwicz and H. Uzawa, *Studies in Linear and Non-Linear Programming*. CA, US: Stanford University Press, 1958.
- [23] A. Rantzer, "Dynamic dual decomposition for distributed control," in *Proc. of American Control Conference*, St. Louis, MO, USA, June 2009.
- [24] D. Feijer and F. Paganini, "Stability of primal-dual gradient dynamics and applications to network optimization," *Automatica*, vol. 46, no. 12, 2010, pp. 1974-1981.
- [25] P. J. Douglass, R. Garcia-Valle, P. Nyeng, J. Ostergaard and M. Togeby, "Smart demand for frequency regulation: Experimental results," *IEEE Transactions on Smart Grid*, 2012.
- [26] H. K. Khalil, *Nonlinear Systems*, 2nd ed. NJ, US: Prentice-Hall, Inc., 1996.